Journal of Automation and Intelligence 4 (2025) 145–159

Contents lists available at ScienceDirect

Journal of Automation and Intelligence


Research article

# Grey wolf optimization-based fuzzy-PID controller for load frequency control in multi-area power systems


Md. Faiyaj Ahmed Limon [a,b,*], Rhydita Shahrin Upoma [a], Nomita Sinha [a], Shristi Roy Swarna [a], Bidyut Kanti Nath [b], Kulsuma Khanum [b], Md. Jubaer Rahman [c], Md. Shahid Iqbal [a,c]

[a] Department of Electrical & Electronic Engineering, Sylhet Engineering College, Sylhet, 3100, Bangladesh
[b] Department of Electrical and Electronic Engineering, Leading University, Sylhet, 3112, Bangladesh
[c] Department of Electrical & Electronic Engineering, Dhaka University of Engineering & Technology, Gazipur, 1707, Bangladesh

ARTICLE INFO

*Keywords:*
Fuzzy-PID controller
Grey wolf algorithm
Load frequency
Triangular membership function
ITAE

ABSTRACT

This study develops a GWO-optimized cascaded fuzzy-PID controller with triangular membership functions for load frequency control in interconnected power systems. The controller's effectiveness is demonstrated on thermal–thermal and hybrid thermal–hydro–gas power systems. The controller parameters were tuned using the Integral Time Absolute Error (ITAE) objective function, which was also evaluated alongside other objective functions (IAE, ISE, and ITSE) to ensure high precision in frequency stabilization. To validate the effectiveness of the triangular membership function, comparisons were made with fuzzy-PID controllers employing trapezoidal and Gaussian membership functions. Performance metrics, including ITAE, settling time, overshoot, and undershoot of frequency deviation, as well as tie-line power deviation, were evaluated. Robustness was established through a comprehensive sensitivity analysis with $T_G$, $T_T$, and $T_R$ parameter variations (±50%), a non-linearity analysis incorporating Generation Rate Constraint (GRC) and Governor Deadband (GDB), a random Step Load Perturbation (SLP) over 0–100 s, and also Stability analysis of the proposed scheme is conducted using multiple approaches, including frequency-domain analysis, Lyapunov stability theory, and eigenvalue analysis. Additionally, the system incorporating thermal, hydro, and gas turbines, along with advanced components like CES and HVDC links, was analysed. Comparisons were conducted against controllers optimized using Modified Grasshopper Optimization Algorithm (MGOA), Honey Badger Algorithm (HBA), Particle Swarm Optimization (PSO), Artificial Bee Colony (ABC), and Spider Monkey Optimization (SMO) algorithms. Results demonstrate that the GWO-based fuzzy-PID controller outperforms the alternatives, exhibiting superior performance across all evaluated metrics. This highlights the potential of the proposed approach as a robust solution for load frequency control in complex and dynamic power systems.

## 1. Introduction

The effective operation of interconnected power systems relies on the balancing total generation with total load demand, including system losses. As the operating conditions of a power system change over time, there can be deviations in the nominal system frequency and planned power exchanges with other regions, which can have negative impacts [1]. Load Frequency Control (LFC), also known as Automatic Generation Control (AGC), is essential in the design and operation of electric power systems, ensuring the delivery of sufficient and reliable high-quality electricity [2]. The deregulation of the power industry and the introduction of large-capacity, fast-responding power equipment are causing significant issues with frequency oscillations. As a result, LFC is becoming increasingly crucial in managing the complexities of interconnected power systems [3].

As interconnected systems have expanded, LFC has become more crucial, enabling the operation of these complex networks. Even today, it remains fundamental to many advanced strategies for managing large-scale systems [4]. In recent decades, numerous studies on load frequency control in interconnected power systems have been published in academic literature. Proportional plus integral (PI) [5,6] and proportional plus integral plus derivative (PID) [7,8] controllers remain the most popular in industrial applications because of their simplicity, straightforward construction and implementation, affordability, and substantial stability margin. In [9], authors introduced a PID controller optimized by the Lozi map-based chaotic algorithm (LCOA)

to tackle the LFC issue, conducting a comparative study to establish the LCOA algorithm's enhanced performance. Another study [10] proposed a PSO-optimized proportional–integral–derivative (PID) controller coordinated with redox flow batteries (RFBs) to improve the LFC of a power system with a significant integration of wind power generation. Additionally, for standalone Multi-Source Power Systems, a PSO-optimized PID controller [11] has been utilized, supported by four different cost functions: IAE, ISE, ITAE, and ITSE. In this context, new strategies have been suggested where two robust decentralized proportional integral (PI) control designs are proposed for LFC, accommodating communication delays. However, these controllers also exhibit inherent disadvantages, such as nonlinearity and sensitivity to parameter changes in dynamic systems. In the domain of load frequency control (LFC), introduces cascaded controllers are emerging as a powerful solution. Notably, a modified cascaded Dual-Loop Linear Active Disturbance Rejection based Tilted controller has been proposed, optimized using a novel Chaotic Quasi-Opposition Crayfish Optimization algorithm (CQOCOA). This controller focuses on optimizing parameters with Integral Time Squared Error (ITSE) as the objective function, providing a detailed examination and successful implementation that signifies a step forward in LFC system design [12]. Consequently, various alternative controllers have been explored in the literature for managing load frequency. These include the fractional order PID (FOPID) controller [13], the fractional-order proportional derivative with a (one plus fractional order integrator) (FOPD-(1+FOI)) cascade controller [14], Exponential PID [15] and the PD–PI cascade control [16],(1+PD)-PID cascade controller [17] and Cascaded (1+PI)-PI-PID Controller [18]. Expanding on innovative control strategies, this work also introduces a fuzzy 1 + proportional + derivative-tilt + integral (F1PD-TI) controller, specifically designed for AGC in power systems featuring renewable energy sources based on solar thermal, wind, and fuel cells. This controller was initially tested on a two-area reheat thermal power system, subsequently applied to a multi-source two-area hydro-thermal power system, showing promising results in both scenarios [19]. A cascade fractional-order integral-derivative and tilt controller tailored [20] for a two-area interconnected hybrid power system that includes thermal, hydro, and gas plants. This system design, which also integrates intermittent solar and wind power as well as electric vehicles, uses a newly modified Quasi-Opposition Reptile Search Algorithm (QORSA) for optimal parameter tuning. The efficacy of this novel controller has been compared against several established meta-heuristic algorithms, demonstrating its superiority and validating the effectiveness of the proposed method. The performance of these controllers has been assessed in single, dual, and triple-area interconnected power systems, which integrate various generation units such as thermal, hydro, and gas turbines.

As the complexity of interconnected power systems grows, traditional controllers like PI and PID, while still prevalent due to their simplicity and reliability, are increasingly being supplemented by advanced fuzzy-PID controllers and algorithms to address the dynamic challenges of load frequency control. In load frequency control (LFC) research, the fuzzy-PID controller has drawn significant interest. In [21], the authors developed a two-layered fuzzy controller to mitigate frequency and tie-line power oscillations under various load conditions. Similarly, [22] proposed a multi-stage fuzzy (PSOMSF) controller to tackle the LFC challenge. To simplify design and enhance performance, a Fuzzy PI controller was created using a hybrid of genetic algorithm and particle-swarm optimization, known as FPI–HGAPSO [23]. Additionally, a hybrid controller combining Local Unimodal Sampling (LUS) and Teaching Learning Based Optimization (TLBO) with a fuzzy-PID configuration was introduced for LFC in a two-area interconnected multi-source power system, with and without an HVDC link. This system includes a reheat thermal unit, a hydro unit, and a gas unit in each area, and the performances of both fuzzy-PID and traditional PID controllers were evaluated [24]. Furthermore, an Adaptive Neuro Fuzzy Inference System (ANFIS) controller was designed for a power network with nonlinearities such as boiler dynamics, generation rate constraint, governor dead-band, and time delay, showing that the ANFIS controller outperforms conventional controllers in peak overshoot and settling time [25]. A hybrid fuzzy proportional derivative–tilt integral derivative (FPD-TID) controller was also introduced for the LFC analysis of a standalone microgrid system, with operational stability confirmed under various scenarios through eigenvalue and root locus analysis [26]. Additionally, a robust fuzzy LFC controller was developed utilizing the robust fuzzy logic-based fine-tuning (RFLFT) approach, aimed at enhancing frequency regulation effectiveness [27]. In [28], authors developed an Improved Ant Colony Optimization (IACO) algorithm optimized fuzzy PID (FPID) controller, incorporating a modified objective function that utilizes integral time multiplied by absolute error (ITAE), as well as metrics for overshoot undershoot, and settling time, each assigned appropriate weight coefficients. This approach aims to enhance the controller's performance. A Hybrid Microgrid System, which includes photovoltaic (PV) and wind energy sources using actual irradiance and wind speed data, employs the proposed FPIDF controller to improve both the frequency stability and tie-line deviation. In a paper introduces a novel fuzzy 1 + proportional + derivative–proportional + integral (F1PD–PI) controller aimed at enhancing the Area Generation Control (AGC) performance across Integrated Power Systems (IPSs) integrating renewable energy sources such as wind, solar, and fuel cells. The design of this controller ingeniously integrates the benefits of fuzzy logic, 1PD, and PI controllers to optimize the balance between generation and load demands. The optimization of the controller's gains and fuzzy membership functions is effectively handled using the Salp Swarm Algorithm (SSA), demonstrating a unique approach to improving AGC performance [29]. Another fuzzy-PID controller [30] has been proposed with spider monkey optimization (SMO), where thermal–thermal power system has been analysed with two conditions without nonlinearity and with nonlinearity.

Expanding on the progress and varied applications of fuzzy-PID controllers in multiple power systems, subsequent research has investigated the integration of these controllers with various algorithms and renewable energy sources to improve system stability and performance. In [31], a fuzzy PID controller utilizing a sine cosine algorithm is proposed for Load Frequency Control (LFC) in a hybrid renewable energy system. Similarly, [32] employs a sine cosine algorithm-based fuzzy PID controller to manage LFC in a three-area system with nonlinear dynamics. Gonggui Chen et al. [28] examined the use of a fuzzy PID controller in a hydrothermal power system encompassing two areas and four sources, assessing performance with and without a High Voltage Direct Current (HVDC) link. In [33], a three-area power system combines conventional energy sources with renewables like solar, biomass, and fuel cells, achieving stability through a Thyristor Controlled Phase Shifter (TCPS) in series with the tie-line, and maintaining power quality for LFC using a supercapacitor energy storage system and a PID controller. Moreover, Capacitive Energy Storage (CES) and a Static Synchronous Series Compensator (SSSC) have been employed for load frequency control in a two-area system comprising thermal, hydro, and gas turbine power sources. The PID controller in this setup was fine-tuned using a hybrid Particle Swarm Optimization (PSO) and Gravitational Search Algorithm (GSA) as reported in [34], as well as a modified Artificial Bee Colony and Particle Swarm Optimization algorithm (MHABC-PSO) detailed in [7].

While the concept of using Grey Wolf Optimization (GWO) to tune fuzzy PID controllers for Load Frequency Control (LFC) is present in literature [35,36], these previous works often focus on improving the GWO itself or modifying the fuzzy-PID controller structure without explicitly investigating the impact of different membership functions, particularly triangular, on the controller's performance. This research introduces a novel approach by employing a cascaded fuzzy-PID controller and uniquely leveraging triangular membership functions within the fuzzy logic system. Prior works often focus on standard fuzzy-PID structures with other membership functions or hybrid controllers with

different tuning methods. This specific combination, as well as the rigorous analysis performed, which includes the membership function impact, distinguishes this work.

This research presents a novel application of a GWO-based cascaded fuzzy-PID controller, specifically employing triangular membership functions within its fuzzy logic component, for load frequency control in a two-area power system. Our proposed control scheme is detailed in Fig. 1. The main contributions of this paper are as follows:

1. Developed a fuzzy-PID controller using Grey Wolf Optimization (GWO) with a Triangular membership function. The controller was designed for two interconnected systems: (i) a Thermal–Thermal system (system 1) and (ii) a combination of Thermal, Hydro, and Gas turbine (system 2). This study used ITAE objective functions for tuning the proposed controller by comparing with others existing objective functions.
2. Compared the performance of the triangular membership function with two distinct fuzzy membership functions—Trapezoidal and Gaussian. These functions were evaluated based on their performance in terms of ITAE, settling times, overshoot, and undershoot of frequency deviation across two areas, as well as power deviation in the tie-line.
3. Conducted three distinct types of studies in system 1—Sensitivity Assessment, Non-linearity Analysis,Random SLP, and Stability analysis to demonstrate the strength and resilience of the proposed control scheme.
4. Examined the robustness of the proposed control scheme in a practical scenario, including a complex power generation system with thermal, hydro, and gas turbine systems, along with CES and HVDC links.
5. Demonstrated the effectiveness of the GWO-based fuzzy-PID controller by comparing it with MGOA, HBA, PSO, ABC, and SMO-based fuzzy-PID controllers.

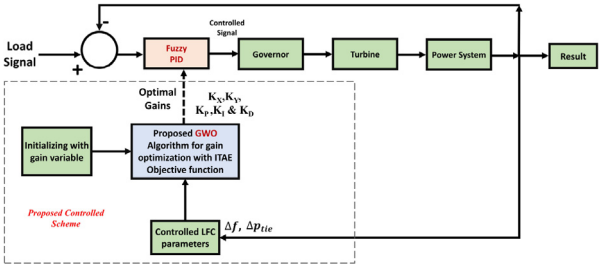


**Fig. 1.** Proposed controlled scheme for two area power system.

## 2. Systems of interest

Primarily, the two-area thermal–thermal power plant (System-1), illustrated in Fig. 2, has been used for designing and evaluating the proposed control scheme. $T_{G1}$ and $T_{G2}$ denote the speed governor time constants in seconds, while $\Delta P_{G1}$ and $\Delta P_{G2}$ represent the changes in governor valve positions (per unit). $T_{T1}$ and $T_{T2}$ are the turbine time constants in seconds, and $\Delta P_{T1}$ and $\Delta P_{T2}$ indicate the changes in turbine output power. $\Delta P_{D1}$ and $\Delta P_{D2}$ correspond to the changes in load demand, and $\Delta P_{Tie}$ represents the incremental change in tie line power (per unit). $K_{P1}$ and $K_{P2}$ stand for the power system gains, and $T_{P1}$ and $T_{P2}$ are the power system time constants in seconds. $T_{12}$ is the synchronizing coefficient, and $\Delta F_1$ and $\Delta F_2$ are the system frequency deviations in Hz. The system is extensively utilized in literature for designing and analysing automatic load frequency control in interconnected areas [30]. In Fig. 2, $B_1$ and $B_2$ denote the frequency bias parameters, while $ACE_1$ and $ACE_2$ represent the area control errors. The control outputs from the controller are indicated by $u_1$ and $u_2$. $R_1$ and $R_2$ are the governor speed regulation parameters in per unit Hertz (pu Hz). The relevant parameters are detailed in Appendix A.

Following that, another system (System-2) was analysed, which is a two-area thermal, hydro, and gas turbine power system equipped with an HVDC link. Additionally, a capacitive energy storage (CES) unit has been integrated into the area. Fig. 3 illustrates this system, while Fig. 2 shows that the regulation parameters for the thermal, hydro, and gas generating units are denoted as $R_1$, $R_2$, and $R_3$, respectively. The control outputs for these units are denoted as $U_T$, $U_H$ and $U_G$, while the participation factors are represented as $K_T$, $K_H$, and $K_G$. The time constants for the thermal, steam, and gas turbine units are indicated as $T_{SG}$, $T_T$, and $T_r$ in seconds. In this power system, the combined participation factors of all these units in a control area must sum to one. Test system 2's relevant parameters are detailed in Appendix B [7,32].

Capacitive Energy Storage (CES) systems are essential for maintaining power system stability by rapidly managing power fluctuations. The CES transfer function model is illustrated in Fig. 4. CES systems process input frequency deviations through several stages: compensators adjust the frequency response, a gain factor modifies the control signal magnitude, and a filter smooths high-frequency components. The final output represents the power change that CES supplies to or absorbs from the grid, thereby regulating system frequency, enhancing power quality, and supporting grid stability. Additionally, CES systems facilitate the integration of renewable energy sources by managing their variability and intermittency.

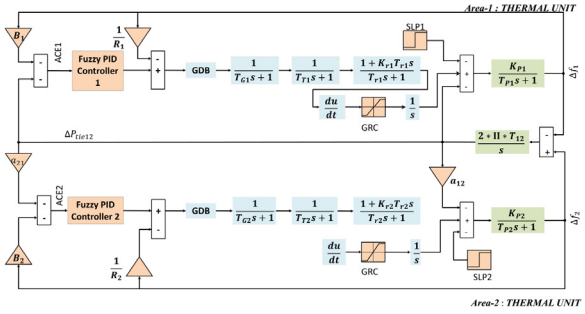


**Fig. 2.** Transfer function of test system 1 with non-linearity.

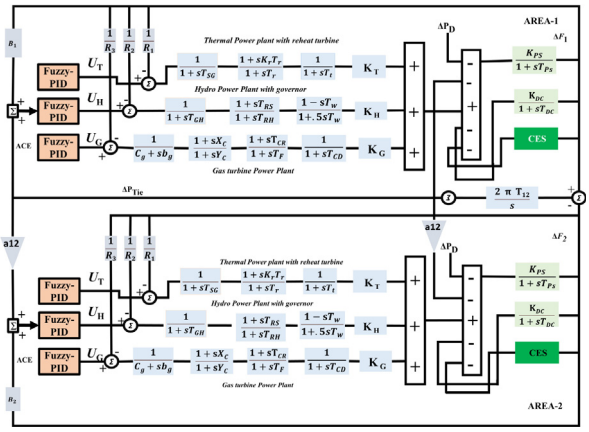


**Fig. 3.** Transfer function of test system 2.

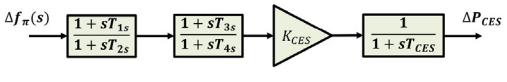

**Fig. 4.** Modelling of capacitive energy storage (CES).

## 3. Proposed controlled scheme

### 3.1. Fuzzy controller structure

In this study, two test systems have been studied with a Fuzzy-PID controller. The structure of the controller is illustrated in Fig. 5 [30,37]. Here, the first two input gains, $K_{Xi}$ and $K_{Yi}$, serve as the scaling factors. Then fuzzy controller is cascaded with PID controller, where $K_{Pi}$, $K_{Ii}$ and $K_{Di}$ are the three gains of PID. These gains of the controller need to be tuned for getting better output. This fuzzy controller receives an input signal, which includes the Area Control Error (ACE) and its derivative, ∇ACE.

The research examined three types of membership functions (MFs): triangular, trapezoidal, and Gaussian as shown in Fig. 6 [38]. These MFs were applied to five fuzzy linguistic variables—large negative (LN), small negative (SN), zero error (ZE), small positive (SP), and large positive (LP)—for both inputs and outputs. For simplicity, this paper employs the Mamdani fuzzy inference engine and the centre of gravity defuzzification method. The fuzzy logic controller (FLC) output is derived from a two-dimensional rule base that considers error, the derivative of error, and the FLC output, as shown in Table 1 [30].

### 3.2. Objective function

The Load Frequency Control (LFC) in power systems must meet two goals during load disturbances: restoring the steady-state frequency to zero and maintaining the predetermined power transfer values [38]. To achieve these goals with optimal settling time, peak overshoot, and peak undershoot, a suitable objective function must be chosen. In our study, we selected the Integral Time Absolute Error (ITAE) objective function over other options such as Integral Absolute Error (IAE), Integral Squared Error (ISE), and Integral Squared Absolute Error (ISAE) [7]. According to various sources, the ITAE objective function demonstrates greater effectiveness than others in terms of settling times and peak values of frequency deviations and power deviation in the tie-line. Eq. (1) defines the ITAE objective function:

$$\mathrm{ITAE} = \int_0^{T_{\mathrm{sim}}} t.([\Delta f_{\mathrm{area1}} + \Delta f_{\mathrm{area2}} + P_{\mathrm{tie-line}}])\,\mathrm{d}t \tag{1}$$

where, $\Delta f_{\mathrm{area1}}$ and $\Delta f_{\mathrm{area2}}$ are the frequency deviations of area-1 and area-2, respectively, $P_{\mathrm{tie-line}}$ is the power deviation in the tie-line. The time range of simulation is denoted as $T_{\mathrm{sim}}$. This objective function was used to tune the controller values with different techniques. A lower ITAE value indicates better performance. It should be noted that all comparative techniques were also tuned using the same objective function.

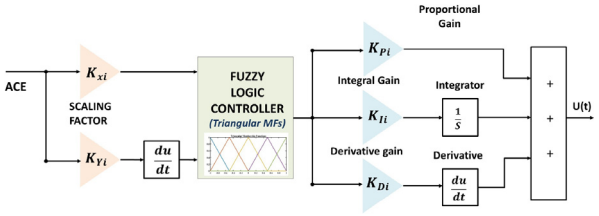


**Fig. 5.** Proposed Fuzzy-PID controller structure.

**Table 1**
Rule base for error, change in error, and fuzzy logic controller output.

| ACE | ΔACE | | | | |
|---|---|---|---|---|---|
| | LN | SN | ZE | SP | LP |
| LN | LN | LN | SN | SN | ZE |
| SN | LN | SN | SN | ZE | SP |
| ZE | SN | SN | ZE | SP | SP |
| SP | SN | ZE | SP | SP | LP |
| LP | ZE | SP | SP | LP | LP |

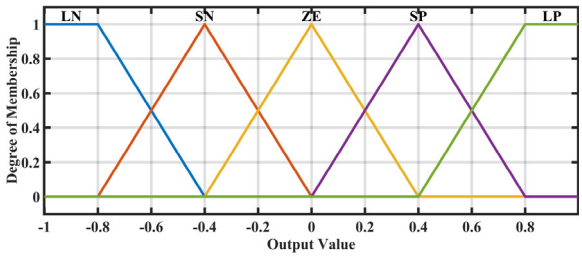


(a)

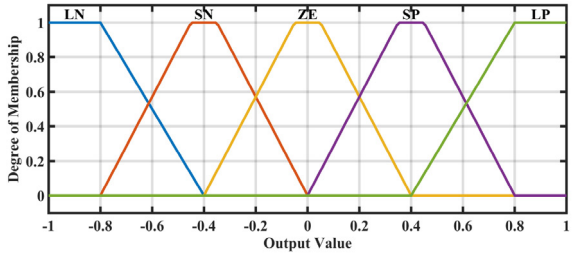


(b)

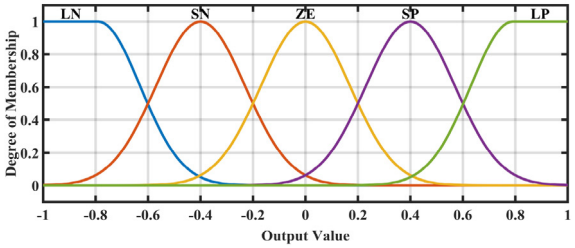


(c)

**Fig. 6.** Three membership function: (a) Triangular; (b) Trapezoidal; (c) Gaussian.

### 3.3. Grey wolf optimization algorithm

The grey wolf (Canis lupus), a prominent member of the Canidae family, is renowned for its prowess as a top predator in the animal kingdom. These wolves typically thrive in packs comprising 5 to 12 individuals, where they exhibit a sophisticated social structure that governs their cooperative behaviours and decision-making processes. This organized hierarchy enables them to efficiently hunt prey and adapt to their environment. The Grey Wolf Optimizer (GWO) algorithm systematically replicates these principles to address optimization problems. It draws inspiration from the grey wolf's hunting tactics and social dynamics. The GWO algorithm employs a series of structured phases that mimic the wolves hierarchical leadership and strategic hunting techniques. Flowcharts illustrating these phases are depicted in Fig. 7, providing a visual representation of how the algorithm progresses through its steps. Each phase, from initialization to exploitation and convergence, is meticulously designed to optimize solutions by leveraging principles derived from the natural behaviours of grey wolves. Key equations underpinning each step ensure that the algorithm navigates the search space effectively, aiming to converge towards optimal solutions akin to how grey wolves collaborate and adapt in their pack dynamics.

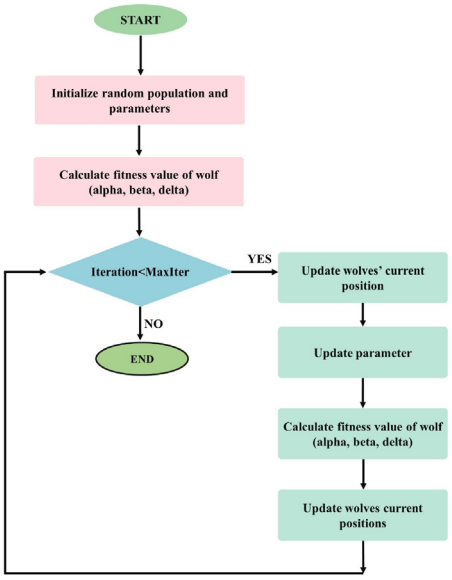


**Fig. 7.** Flowchart of GWO algorithm.

#### 3.3.1. Initialize the population

Create a population of (n) grey wolves randomly distributed in the search space. Each wolf's position represents a potential solution. Position Vector: Each wolf's position is represented as

$$Xi = (xi_1, xi_2, \ldots, xi_d) \tag{2}$$

where, $d$ is the dimensionality of the problem, and $i = 1, 2, \ldots, n$ (number of wolves). After that, set the maximum number of iterations ($T$) that the algorithm will execute, defining the total computational effort. Next, initialize the control parameter ($a$), which starts at 2 and linearly decreases to 0 throughout the iterations, balancing exploration and exploitation. Additionally, update the coefficient vectors ($\boldsymbol{A}$) and ($\boldsymbol{C}$) in each iteration. These parameters guide the wolves' search behaviour and are crucial for convergently on optimal solutions. For the specific equations used to update these parameters, refer to the original work by Mirjalili et al. (2014) [39].

#### 3.3.2. Encircling the prey

In the GWO algorithm, encircling the prey is a crucial step that simulates the natural behaviour of grey wolves as they surround their target. This behaviour is mathematically modelled to ensure that the search agents (wolves) converge towards the best solutions identified so far.

*A. Distance calculation explanation:* The distance between a wolf and the prey (best solution) is calculated. The positions of the prey are represented by the alpha ($\alpha$), beta ($\beta$), and delta ($\delta$) wolves, which are the best three solutions found so far. For each wolf, the distance to the prey (i.e., the alpha, beta, and delta wolves) is calculated. This can be described by the equation:

$$D = \left|\boldsymbol{C} \cdot \boldsymbol{X}^* - \boldsymbol{X}\right| \tag{3}$$

*B. Position update:* Wolves update their positions based on the positions of these three leading wolves. The equations for this process involve two coefficient vectors $\boldsymbol{A}$ and $\boldsymbol{C}$, which dynamically adjust the wolves' positions. The new position of a wolf is then updated by:

$$\boldsymbol{X}(t+1) = \boldsymbol{X}^* - \boldsymbol{A} \cdot D \tag{4}$$

Here, $\boldsymbol{A}$ is another coefficient vector that controls the step size and direction of the movement towards the prey. The vectors $\boldsymbol{A}$ and $\boldsymbol{C}$ are updated in each iteration to fine-tune the balance between exploration and exploitation.

#### 3.3.3. Hunting the prey

In the GWO algorithm, once the prey is encircled, the wolves enter the hunting phase, during which they strive to capture the prey. Each wolf adjusts its position by determining its distances from the alpha, beta, and delta wolves using Eq. (5). Based on these distances, each wolf updates its position by moving closer to the alpha, beta, and delta wolves, with the new positions determined by Eq. (6).

$$\begin{aligned} D_\alpha &= \left|\boldsymbol{C}_\alpha \cdot \boldsymbol{X}_\alpha - \boldsymbol{X}\right|; \\ D_\beta &= \left|\boldsymbol{C}_\beta \cdot \boldsymbol{X}_\beta - \boldsymbol{X}\right|; \\ D_\delta &= \left|\boldsymbol{C}_\delta \cdot \boldsymbol{X}_\delta - \boldsymbol{X}\right| \end{aligned} \tag{5}$$

$$\begin{aligned} \boldsymbol{X}_1 &= \boldsymbol{X}_\alpha - \boldsymbol{A}_\alpha \cdot D_\alpha; \\ \boldsymbol{X}_2 &= \boldsymbol{X}_\beta - \boldsymbol{A}_\beta \cdot D_\beta; \\ \boldsymbol{X}_3 &= \boldsymbol{X}_\delta - \boldsymbol{A}_\delta \cdot D_\delta \end{aligned} \tag{6}$$

Here, $\boldsymbol{X}_\alpha$, $\boldsymbol{X}_\beta$, and $\boldsymbol{X}_\delta$ represent the positions of the alpha, beta, and delta wolves, respectively. $\boldsymbol{C}_\alpha$, $\boldsymbol{C}_\beta$, and $\boldsymbol{C}_\delta$ are coefficient vectors that introduce randomness and influence the search. $\boldsymbol{A}_\alpha$, $\boldsymbol{A}_\beta$, and $\boldsymbol{A}_\delta$ are coefficient vectors that adjust the movement magnitude and direction towards each leading wolf.

Lastly, the wolf's position is updated by averaging the new positions relative to the alpha, beta, and delta wolves:

$$\boldsymbol{X}_{(t+1)} = \frac{\boldsymbol{X}_1 + \boldsymbol{X}_2 + \boldsymbol{X}_3}{3} \tag{7}$$

This averaging ensures that each wolf moves towards a balanced position influenced by the best solutions identified.

#### 3.3.4. Attacking the prey

In the GWO algorithm, the phase after hunting is described as attacking the prey, during which the wolves concentrate on refining and exploiting the best solutions found so far. During this phase, the parameter $a$ linearly decreases from 2 to 0 over the iterations, reducing the influence of random exploration and enhancing the wolves' convergence towards optimal solutions. This decrement in $a$ directs the coefficient vectors $\boldsymbol{A}$ and $\boldsymbol{C}$ to refine the wolves' movements more precisely towards the positions of the alpha, beta, and delta wolves, which represent the top solutions. The wolves update their positions accordingly, aiming to exploit the identified optimal regions by calculating distances and adjusting their movements based on the leading wolves. This focused exploitation phase ensures that the algorithm efficiently converges towards the global optimum, refining the search space and improving solutions iteratively [40].

#### 3.3.5. Termination criteria

The algorithm defines stopping criteria to terminate. It stops when reaching a maximum number of iterations or achieving convergence (e.g., minimal improvement in solutions).

## 4. Result and analysis

### 4.1. Parameters settings

To tune the parameters of the system, we employ the GWO algorithm, which is designed to minimize the fitness value of the objective function under simulated disturbances. In this context, the controller gains for both areas are symmetrical. Hence, each controller has five gains, leading to a search space defined by five variables (nVar = 5) for Test System 1 and fifteen variables (nVar = 15) for Test System 2. The ranges for these controller gains are shown in Table 2, which applies to both test systems. Although Test System 2 uses six Fuzzy-PID controllers, the gain ranges are consistent for each controller.

The GWO algorithm operates with a population of 20 wolves (noW = 20). The initial positions of these wolves are randomly generated within the specified bounds, ensuring diverse initial solutions. The convergence rate parameter 'a' decreases linearly from 2 to 0 over

**Table 2**
Upper and Lower bounds of the controller for Test System 1 and 2.

| Parameter | Description | Lower bound | Upper bound |
|---|---|---|---|
| $K_{Xi}$ | Input gain 1 | 0.1 | 2.0 |
| $K_{Yi}$ | Input gain 2 | 0.1 | 2.0 |
| $K_{Pi}$ | Proportional gain | 0.1 | 2.0 |
| $K_{Ii}$ | Integral gain | 0.1 | 2.0 |
| $K_{Di}$ | Derivative gain | 0.1 | 2.0 |

the iterations, facilitating enhanced exploration in the early stages and exploitation in the later stages. The optimization process is set to iterate for a maximum of 50 iterations (maxIter = 50). The simulation concludes when the stopping criterion of maximum iterations is met.

In this study, the settling times, overshoot, and undershoot of three curves—namely, the frequency deviation in Area 1 ($\Delta f_1$), Area 2 ($\Delta f_2$), and the tie-line power deviation ($\Delta P_{tie}$)—are the main parameters of assessment. The time response specifications for these deviations are critical metrics for assessing controller performance. The system's response is analysed based on settling time, overshoot, and undershoot, within a tolerance band of ±0.1 Hz for $\Delta f_1$ and $\Delta f_2$, and a ±0.025 MW tolerance band for $\Delta P_{tie}$ [41]. These tolerance bands are crucial as they help ensure that the system stabilizes within acceptable limits after disturbances, reflecting the effectiveness and precision of the control strategy employed.

### 4.2. Objective functions performance

In this analysis, we explore the efficacy of various objective functions for optimizing a Fuzzy-PID controller in response to a 1% Step Load Perturbation in Area 1. The objective functions considered are Integral Absolute Error (IAE), Integral Square Error (ISE), Integral Time Square Error (ITSE), and Integral Time Absolute Error (ITAE), with a particular emphasis on the merits of ITAE for this study.

The performance assessment, depicted in Fig. 8 for System 1, demonstrates that the ITAE objective function results in significantly faster settling times compared to other metrics. This rapid response is critical for maintaining system stability and efficiency following disturbances, making ITAE a standout choice for applications that demand swift stabilization. Comparative data provided in Table 3 details the settling times, maximum overshoot, and minimum undershoot for each objective function across three different system areas—Area 1, Area 2, and the Tie-line. Here, ITAE not only shows the shortest settling times (1.4958 s for Area 1, 1.3301 s for Area 2, and 1.4805 s for the Tie-line) but also maintains competitive values for both maximum and minimum settle, highlighting its balanced performance. These results underscore ITAE's effectiveness in reducing the duration of system instability, thereby enhancing the operational safety and efficiency of the control scheme.

Conclusively, the analysis robustly supports ITAE as the optimal objective function for this Fuzzy-PID control scheme, particularly for dynamic environments where quick adjustments are essential for system integrity and performance. ITAE's ability to rapidly return the system to a steady state post-disturbance positions it as the preferred choice in scenarios where minimizing response time is crucial for operational success.

### 4.3. Dynamic analysis with system 1

#### 4.3.1. GWO algorithm with three membership functions

In this section, thermal–thermal power system (Test system-1) has been analysed with 1% slp in Area 1. Firstly, for Fuzzy-PID controller we studied three membership functions with GWO algorithm, to understand which membership function performs with proposed controlled strategy. In Table 4 shows the GWO tuned controller gains for proposed controller with Triangular, Trapezoidal, Gaussian membership functions (MFs) with ITAE value. The Triangular MF ITAE value (0.0053)

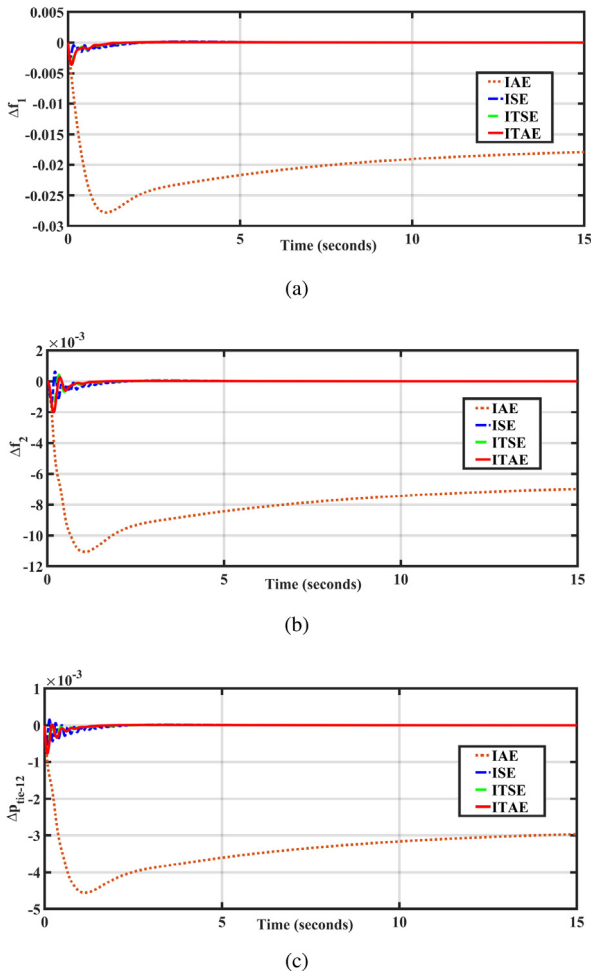


**Fig. 8.** (a) Frequency deviation in area-1; (b) Frequency deviation in area-2; (c) Tie-line Power deviation, with 1% SLP within area-1 in system 1 for different objective functions.

is approximately 49.0% lower than the Trapezoidal MF ITAE value (0.0104) and about 71.9% lower than the Gaussian (MF) ITAE value (0.0189).

Fig. 9 shows the deviation of frequency two areas and power deviation of tie-line for those membership functions. Those curves Settling times ($T_S$), Undershoot ($U_{SH}$) and Overshoot ($O_{SH}$) of GWO based three MFs alongside Spider Monkey Optimization (SMO) based same three MFs for similar conditions are demonstrated in Table 5. The comparison of the Grey Wolf Optimization (GWO) algorithm's performance across Triangular, Trapezoidal, and Gaussian membership functions reveals clear advantages for the Triangular function across various metrics. For Undershoot ($U_{SH}$), the Triangular function achieves reductions of approximately 24.5% compared to the Trapezoidal and 28.6% compared to the Gaussian for $\Delta f_1$, 23.5% and 24.2% respectively for $\Delta f_2$, and 22.1% and 24.4% respectively for $\Delta p_{tie12}$. Regarding Overshoot ($O_{SH}$), Triangular outperforms Trapezoidal by 54.2% for $\Delta f_1$, 58.6% for $\Delta f_2$ (notably, Trapezoidal performs better here with a 24.6% reduction for $\Delta f_2$), and 6.3% for $\Delta p_{tie12}$, and outperforms Gaussian by 73.2% for $\Delta f_1$, 78.4% for $\Delta f_2$, and 99.5% for $\Delta p_{tie12}$. In terms of Settling Time ($T_S$), the Triangular function achieves faster convergence by approximately 71.1% compared to the Trapezoidal and 79.6% compared to the Gaussian for $\Delta f_1$, 60.3% and 77.6% respectively for $\Delta f_2$, and 64.1% and 78.1% respectively for $\Delta p_{tie12}$.

Similarly, across all membership functions (Triangular, Trapezoidal, and Gaussian), the Grey Wolf Optimization (GWO) algorithm consistently outperformed the Spider Monkey Optimization (SMO) algorithm

**Table 3**
Comparison of objective functions across in test system 1.

| Objective function | Settling time (s) | | | $O_{SH} \times 10^{-3}$ | | | $U_{SH} \times 10^{-3}$ | | |
|---|---|---|---|---|---|---|---|---|---|
| | Area 1 | Area 2 | Tie-line | Area 1 | Area 2 | Tie-line | Area 1 | Area 2 | Tie-line |
| IAE | 13.0098 | 12.9909 | 13.0217 | 17.94 | 7.061 | 3.011 | −27.80 | −11.06 | −4.566 |
| ISE | 5.6493 | 4.7494 | 5.0715 | 0.123 | 0.05306 | 0.01979 | −2.403 | −1.399 | −0.5319 |
| ITSE | 1.746 | 1.5330 | 1.6900 | 0.05822 | 0.4037 | 0.06459 | −3.397 | −1.912 | −0.7269 |
| ITAE | 1.4958 | 1.3301 | 1.4805 | 0.06062 | 0.2478 | 0.01801 | −3.606 | −1.975 | −0.7705 |

**Table 4**
Fuzzy-PID gains values of system with ITAE value for three membership functions.

| Gain | | Triangular | Trapezoidal | Gaussian |
|---|---|---|---|---|
| Area-1 & Area-2 | $K_{X1}$ | 1.9740 | 2.0000 | 1.8310 |
| | $K_{Y1}$ | 0.5610 | 1.2716 | 1.7257 |
| | $K_{P1}$ | 1.4400 | 1.4530 | 2.0000 |
| | $K_{I1}$ | 1.9800 | 1.6904 | 1.9056 |
| | $K_{D1}$ | 0.7660 | 0.5545 | 0.9740 |
| ITAE | | 0.0053 | 0.0104 | 0.0189 |

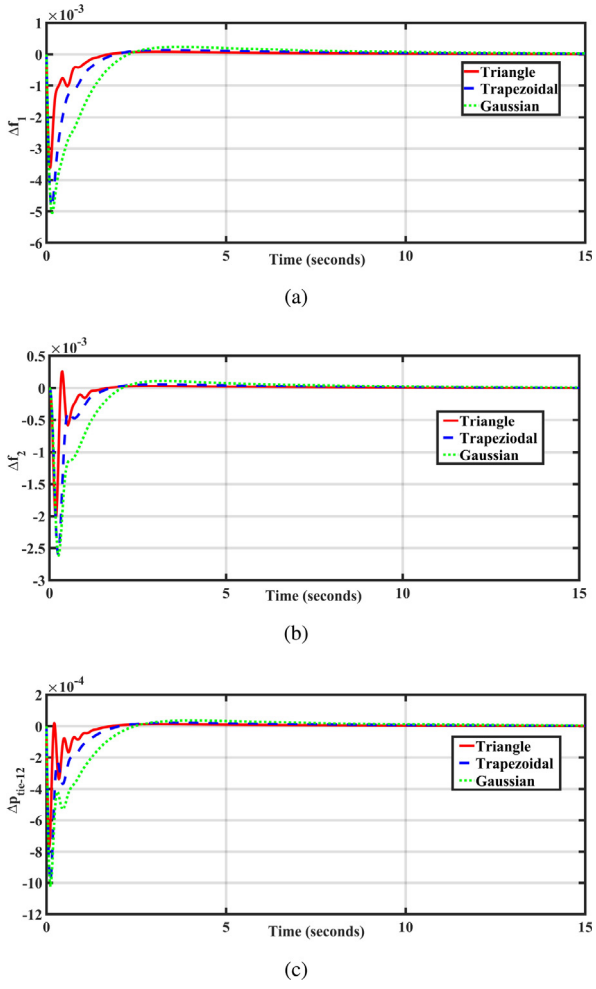


**Fig. 9.** (a) Frequency deviation in area-1; (b) Frequency deviation in area-2; (c) Tie-line Power deviation, with 1% SLP within area-1 in system 1 for Three Membership functions.

in terms of minimizing undershoot, overshoot, settling time, and ITAE. GWO demonstrated superior control performance with notable improvements ranging from 42.3% to 84.9% across different metrics and membership functions. Therefore, GWO is highly recommended for tuning parameters in control systems due to its effectiveness in enhancing both transient response and steady-state accuracy under various operating conditions.

Overall, these results clearly indicate that the Triangular membership function offers superior control performance, with significant improvements in reducing undershoot, overshoot, and settling time, as well as minimizing ITAE, making it the most effective choice among the three for optimizing control system parameters using GWO.

#### 4.3.2. Comparison with other algorithms

The proposed control scheme, a GWO-based Fuzzy-PID controller with a triangular membership function, is compared with PSO, ABC, MGOA, and HBA. Table 6 presents the PID gains of these algorithms along with their respective ITAE values. The Grey Wolf Optimization (GWO) algorithm achieves an ITAE value of 0.0053, significantly outperforming the PSO and ABC algorithms, which record ITAE values of 0.0271 and 0.0320, respectively. Moreover, GWO's ITAE is 80.4% lower than PSO and 83.4% lower than ABC, highlighting its superior ability to minimize error and enhance control performance. Compared to MGOA and HBA, which have ITAE values of 0.0076 and 0.0184 respectively, GWO still demonstrates the best performance, with ITAE reductions of 30.3% compared to MGOA and 71.2% compared to HBA.

Comparison between five algorithms as shown in Fig. 10. The figure depicts frequency deviation of two areas and power deviation of the tie-line for a 1% step load perturbation (SLP) in area 1. Table 7 compares the performance of five algorithms — SMO, PSO, ABC, MGOA, and GWO — on several metrics: settling time, undershoot, overshoot, and the Integral of Time-weighted Absolute Error (ITAE).

The Grey Wolf Optimization (GWO) algorithm excels in all performance metrics. It achieves the shortest settling times with values of 1.4958 s, 1.3301 s, and 1.4805 s for $\Delta f_1$, $\Delta f_2$, and $\Delta p_{\text{tie-12}}$, respectively, outperforming SMO, PSO, ABC, and other evaluated algorithms by significant margins. For undershoot, GWO records the lowest values of −3.606, −1.975, and −0.7705 Hz for $\Delta f_1$, $\Delta f_2$, and $\Delta p_{\text{tie-12}}$, respectively. In terms of overshoot, GWO also shows superior performance with minimal values of 0.06062 Hz, 0.2478 Hz, and 0.01801 Hz. Additionally, GWO achieves the lowest ITAE of 0.0053, marking a significant improvement over PSO (0.0271) and ABC (0.0320), and demonstrating its enhanced ability to minimize cumulative error over time. This comparison clearly indicates that GWO offers superior control performance, making it the most effective algorithm among the six evaluated.

### 4.4. Sensitivity analysis for test system 1

Table 8 shows the sensitivity analysis of the GWO-tuned fuzzy PID controller reveals its superior performance over PSO and ABC controllers across various parameter variations: $T_G$ (Governor Time Constant), $T_T$ (Turbine Time Constant), and $T_R$ (Regulator Time Constant). Settling Time ($T_S$) and Integrated Time Absolute Error (ITAE) were used as performance metrics. Under different $T_G$ variations, the GWO controller consistently exhibited lower $T_S$ and ITAE values compared to PSO and ABC controllers. For instance, with a 50% increase in $T_G$, GWO achieved a $T_S$ of 1.3687 s and ITAE of 0.0053, whereas PSO and ABC controllers showed $T_S$ values of 6.2313 and 8.7302 s, and ITAE values of 0.0288 and 0.0315, respectively. Similarly, a 50% reduction in $T_G$ resulted in GWO maintaining lower $T_S$ and ITAE values compared to PSO and ABC. When $T_T$ and $T_R$ were varied, similar trends were observed. GWO consistently outperformed PSO and ABC controllers with lower settling Time and ITAE values across different levels of $T_T$ and $T_R$ variations. Notably, under extreme variations, such

**Table 5**
Comparison analysis of 3 FIS files with ITAE, settling time, overshoot, and undershoot.

| Membership function | Dynamic analysis | Performance metrics | | | | | |
|---|---|---|---|---|---|---|---|
| | | SMO [30] | | | GWO | | |
| | | Triangular | Trapezoidal | Gaussian | Triangular | Trapezoidal | Gaussian |
| $\Delta f_1$ | $U_{SH} \times 10^{-3}$ in Hz | −6.693 | −9.704 | −11.302 | −3.606 | −4.779 | −5.050 |
| | $O_{SH} \times 10^{-3}$ in Hz | 0.271 | 0.506 | 0.588 | 0.06062 | 0.1323 | 0.2260 |
| | $T_S$ in s | 5.014 | 7.078 | 10.493 | 1.495 | 5.171 | 7.345 |
| $\Delta f_2$ | $U_{SH} \times 10^{-3}$ in Hz | −3.425 | −5.436 | −7.542 | −1.975 | −2.581 | −2.607 |
| | $O_{SH} \times 10^{-3}$ in Hz | 0.164 | 0.351 | 0.398 | 0.2478 | 0.0504 | 0.1081 |
| | $T_S$ in s | 2.718 | 6.734 | 10.83 | 1.330 | 3.353 | 5.9421 |
| $\Delta p_{tie\text{-}12}$ | $U_{SH} \times 10^{-3}$ in Hz | −1.208 | −1.81 | −2.421 | −0.770 | −0.9896 | −1.019 |
| | $O_{SH} \times 10^{-3}$ in Hz | 0.049 | 0.061 | 0.131 | 0.0180 | 0.0193 | 3.503 |
| | $T_S$ in s | 2.374 | 2.85 | 4.294 | 1.4805 | 4.1229 | 6.762 |
| ITAE | | – | | | 0.0053 | 0.0104 | 0.0189 |

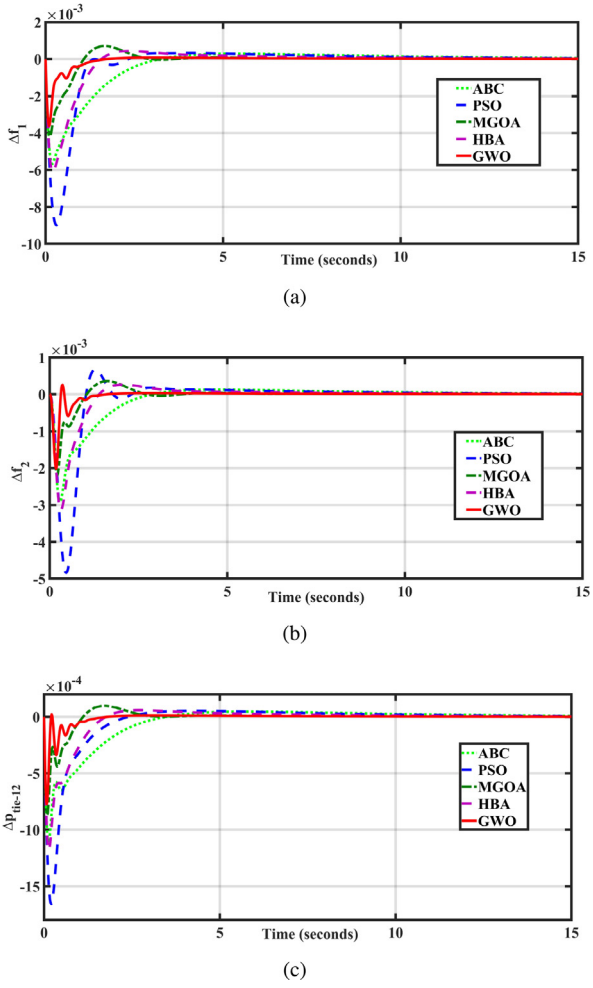


**Fig. 10.** (a) Frequency deviation in area-1; (b) Frequency deviation in area-2; (c) Tie-line Power deviation, with 1% SLP within area-1 in system 1 for different algorithms.

as 50% increases or reductions in $T_T$ and $T_R$, GWO maintained better stability and performance metrics. To demonstrate how settling time varies due to changes in system parameters within the range of +50% to −50%, Fig. 11 illustrates the GWO algorithm's superiority in terms of settling time for variations in (a) $T_G$ (b) $T_T$ and (c) $T_R$ respectively.

In summary, the GWO-tuned fuzzy PID controller demonstrates robustness and superior performance across all parameter variations tested in the sensitivity analysis. These results underscore GWO's effectiveness in achieving faster response times and lower error rates compared to PSO and ABC controllers, making it a promising choice for applications requiring reliable and efficient control systems.

**Table 6**
Fuzzy-PID gains values of the system-1 with ITAE value for five algorithms.

| Gain | Algorithms | Controller gains | | | | |
|---|---|---|---|---|---|---|
| | | GWO | PSO | ABC | MGOA [42] | HBA [43] |
| Area-1 and Area-2 | $K_{X1}$ | 1.974 | 1.6160 | 2.0000 | 1.5823 | 1.9177 |
| | $K_{Y1}$ | 0.5610 | 0.1000 | 2.0000 | 2.0000 | 0.1416 |
| | $K_{P1}$ | 1.4400 | 1.7317 | 2.0000 | 1.5560 | 1.2714 |
| | $K_{I1}$ | 1.980 | 1.9914 | 1.4371 | 1.8832 | 1.7700 |
| | $K_{D1}$ | 0.7660 | 0.2808 | 0.6806 | 0.6918 | 0.4034 |
| ITAE | | 0.0053 | 0.0271 | 0.0320 | 0.0076 | 0.0184 |

### 4.5. Performance analysis with random SLP in area-1 and area-2

In practical power systems, sudden load perturbations (SLP) can occur unexpectedly, necessitating robust control mechanisms to maintain stability. Our proposed controller, designed to perform under such conditions, demonstrates resilience by effectively managing random SLP scenarios, as shown in Fig. 12 for an interconnected power system. As illustrated in Table 9 and Fig. 13, our GWO-tuned Fuzzy PID controller outperforms the PSO and ABC algorithms across various time intervals (0–100 s) in both areas. The results indicate that our controller achieves faster settling times, showcasing its superior ability to adapt to abrupt load changes and ensuring more stable and reliable system performance under both normal and perturbed conditions.

Overall, the GWO-tuned Fuzzy PID controller shows an average improvement of 17.62% over PSO and 15.89% over ABC across all intervals. This consistent enhancement in settling times across different load scenarios and time intervals validates the GWO-tuned controller as a robust and effective solution for managing sudden load perturbations in interconnected power systems, ensuring quicker stabilization and improved system reliability (see Figs. 12 and 13).

### 4.6. Stability analysis with system 1

In this section, the stability analysis of the proposed scheme is conducted using multiple approaches, including frequency-domain, Lyapunov stability theory and eigenvalue analyses. Frequency-domain analysis through the Bode plot Fig. 14(a) reveals a gain margin of 14.78 dB, while the Nyquist plot Fig. 14(b) does not encircle the critical −1 point, both confirming stability. In addition, a pole-zero analysis Fig. 14(c) shows that all poles are in the left-half of the s-plane.

To provide further verification, an eigenvalue analysis was performed. As shown in Table 10, all eigenvalues of matrix $A$, representing the system dynamics, have negative real parts, which aligns with the pole locations and confirms the system's stability. The corresponding eigenvalues of matrix $P$ are all positive, further proving the stability of the system through Lyapunov stability theory.

**Table 7**
Comparison analysis of dynamic performance metrics across different algorithms for system 1.

| Algorithm type | $T_s$ (s) | | | $\lvert U_s \rvert$ (Hz) × $10^{-3}$ | | | $\lvert O_S \rvert$ (Hz) × $10^{-3}$ | | | ITAE |
|---|---|---|---|---|---|---|---|---|---|---|
| | $\Delta f_1$ | $\Delta f_2$ | $\Delta p_{tie-12}$ | $\Delta f_1$ | $\Delta f_2$ | $\Delta p_{tie-12}$ | $\Delta f_1$ | $\Delta f_2$ | $\Delta p_{tie-12}$ | |
| SMO [30] | 5.014 | 2.718 | 2.374 | −6.693 | −3.425 | −1.208 | 0.271 | 0.164 | 0.049 | *N/A* |
| PSO | 6.6325 | 4.8960 | 6.4223 | −8.980 | −4.839 | −1.655 | 0.3018 | 0.6694 | 0.05126 | 0.0271 |
| ABC | 9.2340 | 7.9009 | 8.8135 | −5.656 | −2.882 | −1.114 | 0.2806 | 0.1244 | 0.04424 | 0.0320 |
| MGOA [42] | 2.6927 | 2.5384 | 2.7654 | −4.176 | −2.190 | −0.8677 | 0.7143 | 0.3597 | 0.09757 | 0.0076 |
| HBA [43] | 6.0519 | 4.1619 | 5.5559 | −6.082 | −3.141 | −1.187 | 0.4376 | 0.2660 | 0.05817 | 0.0184 |
| GWO | 1.4958 | 1.3301 | 1.4805 | −3.606 | −1.975 | −0.7705 | 0.06062 | 0.2478 | 0.01801 | 0.0053 |

**Table 8**
Sensitivity analysis with +50% and −50% changes in parameters in area-1 and area-2.

| Parameter | % change | GWO | | | | PSO | | | | ABC | | | |
|---|---|---|---|---|---|---|---|---|---|---|---|---|---|
| | | $T_S$ in S | | | ITAE | $T_S$ in S | | | ITAE | $T_S$ in S | | | ITAE |
| | | $\Delta f_1$ | $\Delta f_2$ | $\Delta p_{\text{tie-12}}$ | | $\Delta f_1$ | $\Delta f_2$ | $\Delta p_{\text{tie-12}}$ | | $\Delta f_1$ | $\Delta f_2$ | $\Delta p_{\text{tie-12}}$ | |
| Nominal values | | 1.50 | 1.33 | 1.48 | 0.005 | 6.63 | 4.90 | 6.42 | 0.027 | 9.23 | 7.90 | 8.81 | 0.032 |
| $T_G$ | +50% | 1.37 | 1.47 | 1.46 | 0.005 | 6.23 | 4.69 | 5.97 | 0.028 | 8.73 | 7.19 | 8.28 | 0.031 |
| | +25% | 1.37 | 1.24 | 1.40 | 0.005 | 6.41 | 4.69 | 6.18 | 0.027 | 8.97 | 7.52 | 8.52 | 0.031 |
| | −25% | 1.42 | 1.39 | 1.52 | 0.005 | 6.87 | 5.24 | 6.70 | 0.027 | 9.54 | 8.33 | 9.14 | 0.032 |
| | −50% | 1.49 | 1.44 | 1.58 | 0.005 | 7.12 | 5.62 | 7.02 | 0.027 | 9.87 | 8.83 | 9.55 | 0.032 |
| $T_T$ | +50% | 1.02 | 0.94 | 1.17 | 0.005 | 5.74 | 5.45 | 5.71 | 0.033 | 8.40 | 6.81 | 8.07 | 0.030 |
| | +25% | 1.32 | 1.23 | 1.33 | 0.005 | 6.17 | 4.91 | 6.03 | 0.029 | 8.79 | 7.34 | 8.41 | 0.031 |
| | −25% | 1.49 | 1.48 | 1.61 | 0.005 | 7.16 | 5.60 | 6.91 | 0.027 | 9.75 | 8.52 | 9.29 | 0.032 |
| | −50% | 1.40 | 1.67 | 1.79 | 0.005 | 7.82 | 6.45 | 7.53 | 0.028 | 10.37 | 9.26 | 9.89 | 0.033 |
| $T_R$ | +50% | 1.60 | 1.45 | 1.57 | 0.005 | 5.19 | 3.20 | 2.39 | 0.029 | 8.55 | 7.16 | 7.59 | 0.035 |
| | +25% | 1.55 | 1.40 | 1.53 | 0.005 | 6.16 | 4.25 | 5.75 | 0.029 | 9.03 | 7.67 | 8.44 | 0.034 |
| | −25% | 2.00 | 2.00 | 1.46 | 0.005 | 5.74 | 4.47 | 4.55 | 0.015 | 8.86 | 7.41 | 7.61 | 0.019 |
| | −50% | 1.99 | 1.99 | 1.59 | 0.005 | 6.70 | 5.53 | 5.72 | 0.014 | 9.35 | 8.13 | 8.34 | 0.019 |

**Table 9**
Settling Time results in the presence of random SLP in area-1 and area-2.

| Different algorithms utilizing cascade controllers | | Time (s) | | | | |
|---|---|---|---|---|---|---|
| | | 0–20 s | 20–40 s | 40–60 s | 60–80 s | 80–100 s |
| Proposed GWO Fuzzy-PID | $F_1$ | 1.6731 | 21.6571 | 41.2663 | 61.6490 | 81.2782 |
| | $F_2$ | 1.6499 | 21.6438 | 41.5670 | 61.6570 | 81.2773 |
| | $P_{tie}$ | 0.5327 | 20.5442 | 40.3528 | 60.3516 | 80.3501 |
| PSO Fuzzy-PID | $F_1$ | 5.8628 | 25.8528 | 41.5616 | 64.9019 | 81.5281 |
| | $F_2$ | 4.6446 | 24.3405 | 41.5600 | 65.6997 | 81.5135 |
| | $P_{tie}$ | 1.7490 | 21.7562 | 41.4982 | 61.4882 | 80.4730 |
| ABC Fuzzy-PID | $F_1$ | 3.6862 | 24.0610 | 41.9727 | 63.9398 | 81.9876 |
| | $F_2$ | 3.9175 | 23.9003 | 42.0237 | 64.0373 | 81.9860 |
| | $P_{tie}$ | 1.9397 | 21.9354 | 41.6842 | 61.6858 | 80.6927 |

**Table 10**
Eigenvalues of $A$ and $P$.

| Eigenvalues of $A$ | Eigenvalues of $P$ |
|---|---|
| $-105.9077 + 0.0000i$ | 0.0044 |
| $-102.6816 + 0.0000i$ | 0.0046 |
| $-4.3899 + 23.3037i$ | 0.0961 |
| $-4.3899 - 23.3037i$ | 0.1401 |
| $-4.2549 + 14.5400i$ | 0.2091 |
| $-4.2549 - 14.5400i$ | 0.2702 |
| $-0.2010 + 0.0000i$ | 1.8404 |
| $-0.1999 + 0.0000i$ | 2.2678 |
| $-2.2961 + 0.2258i$ | 2.7402 |
| $-2.2961 - 0.2258i$ | 2.8981 |
| $-2.1797 + 0.1574i$ | 40.1504 |
| $-2.1797 - 0.1574i$ | 100.5639 |

### 4.7. Non-linearity analysis with system 1

#### 4.7.1. GWO algorithm with three membership functions

In this section, system 1 will be analysed by adding non-linearity, generation rate constraint (GRC), Governor Deadband (GDB) in both areas of the test system [30], which are shown in Fig. 2. With these non-linearities and a 1% SLP in area-1, the tuned values of our GWO algorithms for three membership functions are shown in Table 11 along with ITAE values. The Triangular membership function outperforms the Trapezoidal by 0.79% and the Gaussian by 33.76% in terms of ITAE, indicating superior control performance.

Additionally, a comparison analysis has been made with three membership functions for our proposed GWO algorithm. Fig. 15 and Table 12 shows the result of 1% SLP in area 1, including frequency deviation in both areas and power deviation of the tie-line. The Proposed GWO tuned Fuzzy PID controller works better with a triangular membership function in terms of settling times, overshoot, and undershoot of those deviations. GWO-based Triangular membership functions demonstrate superior overall performance compared to Trapezoidal and Gaussian functions. For instance, the Triangular function achieves a lower frequency deviation of $-17.66\times10^{-3}$ compared to $-17.56\times10^{-3}$ Hz for the Trapezoidal and $-18.26\times10^{-3}$ Hz for the Gaussian. Additionally, the Triangular function maintains a minimal overshoot of $0.7186 \times 10^{-3}$ Hz, outperforming the Trapezoidal at $6.835 \times 10^{-3}$ Hz and the Gaussian at $4.643\times10^{-3}$ Hz. Furthermore, it boasts the shortest settling time of 2.3115 s, faster than both the Trapezoidal at 3.9358 s and the Gaussian at 5.5273 s, underscoring its superior control capabilities.

#### 4.7.2. Comparison with others algorithms

Another table, Table 13, presents the gain values of Fuzzy PID triangular membership functions based on the GWO algorithm, alongside

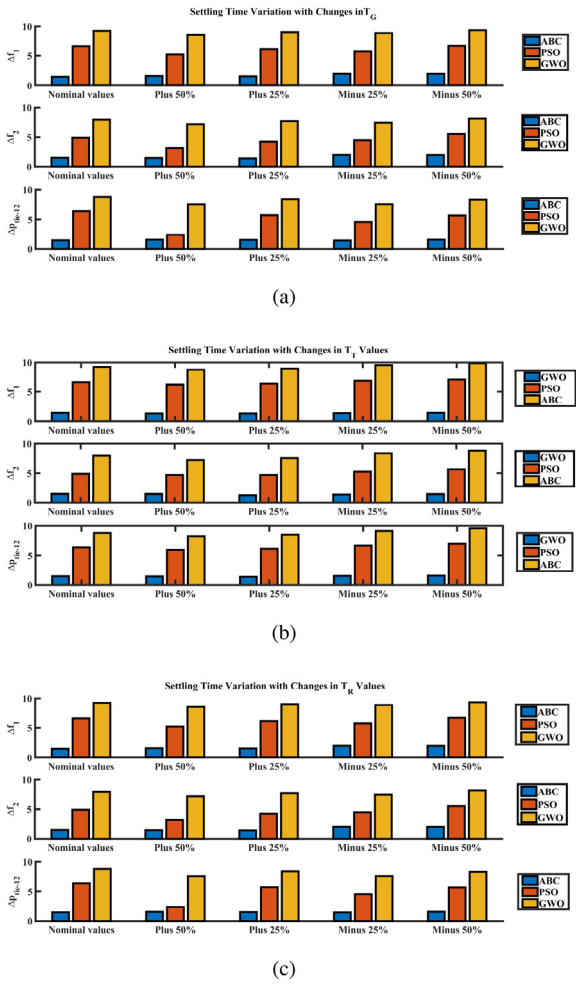


**Fig. 11.** Settling time of frequency deviation in area-1, area-2 and Tie-line Power deviation, with 1% SLP within area-1 with variation in (a) $T_G$; (b) $T_T$; and (c) $T_R$.

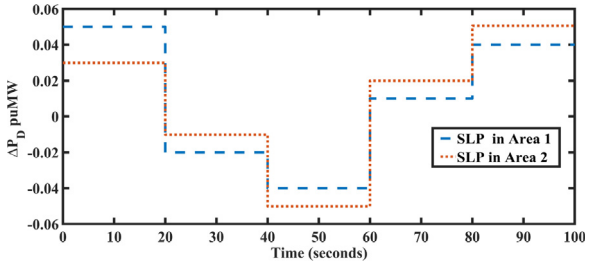


**Fig. 12.** Graphical representation for Random SLP in (a) area-1; (b) area-2.

**Table 11**
Fuzzy-PID gains values of system 1 for non-linearity with ITAE value.

| Gain | GWO | Membership functions | | |
|---|---|---|---|---|
| | | Triangular | Trapezoidal | Gaussian |
| Area-1 and Area-2 | $K_{X1}$ | 1.3932 | 2.0000 | 1.9006 |
| | $K_{Y1}$ | 0.6220 | 1.2010 | 0.6696 |
| | $K_{P1}$ | 2.6039 | 1.1635 | 1.9549 |
| | $K_{I1}$ | 2.4199 | 2.0000 | 1.8710 |
| | $K_{D1}$ | 0.6699 | 0.3300 | 0.3855 |
| ITAE | | 0.0251 | 0.0253 | 0.0382 |

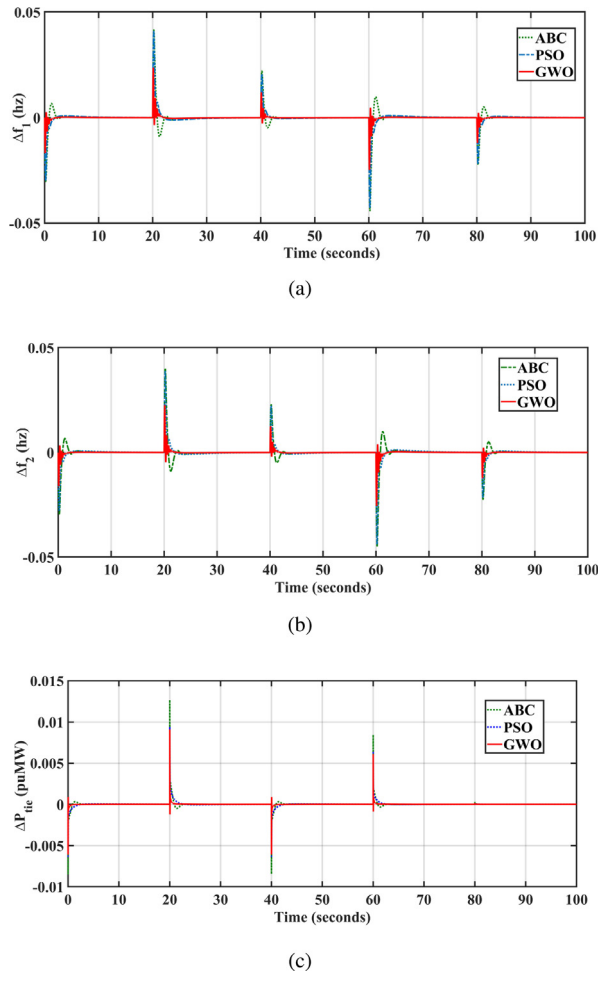


**Fig. 13.** (a) Frequency deviation in area-1; (b) Frequency deviation in area-2; (c) Tie-line Power deviation, with random SLP within area-1 and area-2 for system 1.

PSO, ABC, MGOA, and HBA algorithms. Fig. 16 illustrates the convergence curve for the nonlinear system of these three algorithms, where GWO demonstrates faster convergence than the others. Additionally, Fig. 16 depicts the system's response to a 1% SLP in Area 1, showing that GWO reaches a steady-state position more quickly than the other algorithms. The overall comparison results are shown in Table 14. Among the algorithms compared, GWO stands out as the most effective. It exhibits the lowest settling times ($T_s$) of 2.3115 s, 3.2962 s, and 4.3937 s across $\Delta f_1$, $\Delta f_2$, and $\Delta p_{\text{tie-12}}$ respectively, which represents a significant improvement over the second-best algorithm, PSO, that posts settling times of 6.6951 s, 6.4104 s, and 6.8732 s. Additionally, GWO achieves substantial reductions in undershoot ($U_s$) with values of −17.66 Hz, and in overshoot ($O_s$) with values of $4.643 \times 10^{-3}$ Hz for $\Delta f_1$, highlighting a marked performance improvement. Furthermore, GWO's ITAE score of 0.0251 is the lowest, indicating superior control performance and reduced error compared to PSO's ITAE of 0.0434 and ABC's of 0.1376. While SMO, ABC, and other algorithms show decent performance, their higher settling times and less optimal undershoot and overshoot values make them less favourable compared to GWO, which clearly excels in both efficiency and precision in managing frequency and tie-line power deviations (see Table 12).

### 4.8. Study on system 2

Table 15 presents the gain values for the PID control of System 2 using three different algorithms: GWO, PSO, and ABC, along with their

**Table 12**
Comparison analysis of 3 FIS files with ITAE, settling time, overshoot, and undershoot.

| Membership function | | SMO [30] | | | GWO | | |
|---|---|---|---|---|---|---|---|
| | | Triangular | Trapezoidal | Gaussian | Triangular | Trapezoidal | Gaussian |
| $\Delta f_1$ | $U_{SH} \times 10^{-3}$ in Hz | −10.77 | −13.96 | −17.59 | −17.66 | −17.56 | −18.26 |
| | $O_{SH} \times 10^{-3}$ in Hz | 0.586 | 1.336 | 1.827 | 4.643 | 6.835 | 0.7186 |
| | $T_S$ in s | 6.348 | 6.907 | 12.150 | 2.3115 | 3.9358 | 5.5273 |
| $\Delta f_2$ | $U_{SH} \times 10^{-3}$ in Hz | −4.851 | −8.151 | −9.875 | −2.485 | −2.483 | −2.672 |
| | $O_{SH} \times 10^{-3}$ in Hz | 0.560 | 1.215 | 1.438 | 0.7599 | 1.043 | 0.5561 |
| | $T_S$ in s | 6.169 | 7.710 | 12.827 | 3.2962 | 3.9574 | 5.9560 |
| $\Delta p_{12}$ | $U_{SH} \times 10^{-3}$ in Hz | −1.925 | −2.802 | −4.077 | −0.6703 | −0.6696 | −0.7143 |
| | $O_{SH} \times 10^{-3}$ in Hz | 0.107 | 0.121 | 0.192 | 0.1717 | 0.2547 | 0.02622 |
| | $T_S$ in s | 2.119 | 1.928 | 5.443 | 4.3937 | 3.9139 | 2.7135 |
| ITAE | | – | | | 0.0251 | 0.0253 | 0.0382 |

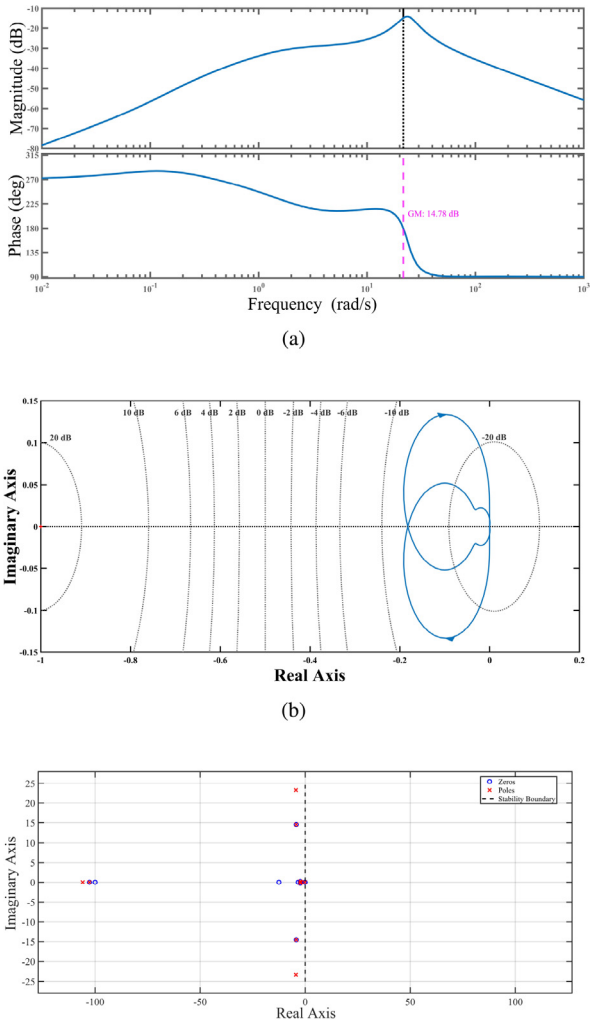


**Fig. 14.** (a) Bode Plot; (b) Nyquist Plot; (c) Pole-Zero plotting.

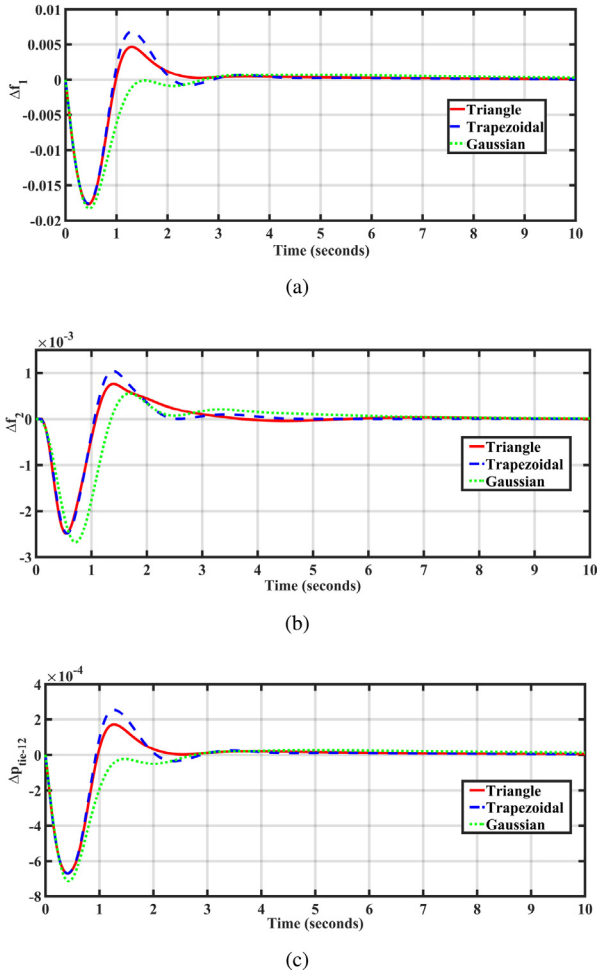


**Fig. 15.** (a) Frequency deviation in area-1; (b) Frequency deviation in area-2; (c) Tie-line Power deviation, with a 1% SLP within area-1 in system 1, incorporating non-linearity, using three different membership functions.

corresponding ITAE values. The table highlights that GWO achieves the most effective tuning, as evidenced by its optimal gain values and the lowest ITAE score of 0.0690. This suggests superior control performance with reduced error compared to PSO and ABC, which have higher ITAE values of 0.1138 and 0.3260, respectively.

Fig. 17 illustrates the system's response to a 1% SLP in Area 1 for System 2, where (a) shows the frequency deviation in Area 1, (b) depicts the frequency deviation in Area 2, and (c) illustrates the tie-line power deviation. The plots in Fig. 17 clearly demonstrate that GWO

**Table 13**
Fuzzy-PID gains values of the system 1 with ITAE value for five algorithms with GRC and GDB.

| Gain | GWO | PSO | ABC | MGOA [42] | HBA [43] |
|---|---|---|---|---|---|
| $K_{X1}$ | 1.3932 | 1.4759 | 1.7296 | 0.2554 | 0.9139 |
| $K_{Y1}$ | 0.6220 | 2.0000 | 0.1000 | 2.0000 | 1.6350 |
| $K_{P1}$ | 1.6039 | 2.0000 | 1.9611 | 1.4210 | 0.7138 |
| $K_{I1}$ | 1.4199 | 2.0000 | 0.3293 | 1.0791 | 0.4332 |
| $K_{D1}$ | 0.6699 | 0.3197 | 0.2174 | 1.3872 | 0.4100 |
| ITAE | 0.0251 | 0.0434 | 0.1376 | 0.1563 | 0.3816 |

**Table 14**
Comparison analysis of dynamic performance metrics across different algorithms for system 1 with non-linearities.

| Algorithm | $T_s$ (s) | | | $\lvert U_s \rvert$ (Hz) × $10^{-3}$ | | | $\lvert O_S \rvert$ (Hz) × $10^{-3}$ | | | ITAE |
|---|---|---|---|---|---|---|---|---|---|---|
| | $\Delta f_1$ | $\Delta f_2$ | $\Delta p_{\text{tie}-12}$ | $\Delta f_1$ | $\Delta f_2$ | $\Delta p_{\text{tie}-12}$ | $\Delta f_1$ | $\Delta f_2$ | $\Delta p_{\text{tie}-12}$ | |
| SMO [30] | 6.348 | 6.169 | 2.119 | −10.77 | −4.851 | −1.925 | 0.586 | 0.560 | 0.107 | *N/A* |
| PSO | 6.6951 | 6.4104 | 6.8732 | −18.04 | −2.568 | −0.6703 | 1.970 | 0.4079 | 0.06879 | 0.0434 |
| ABC | 11.1784 | 9.7171 | 11.1905 | −18.43 | −2.856 | −0.7235 | 0.02719 | 0.6702 | 0.00120 | 0.1376 |
| MGOA [42] | 10.7332 | 10.7453 | 11.3642 | −17.73 | −5.956 | −2.476 | 3.574 | 1.895 | 0.05310 | 0.1563 |
| HBA [43] | 11.3023 | 12.6872 | 12.4523 | −20.85 | −6.757 | −1.646 | 2.244 | 0 | 0 | 0.3816 |
| GWO | 2.3115 | 3.2962 | 4.3937 | −17.66 | −2.485 | −0.6703 | 4.643 | 0.7599 | 0.1717 | 0.0251 |

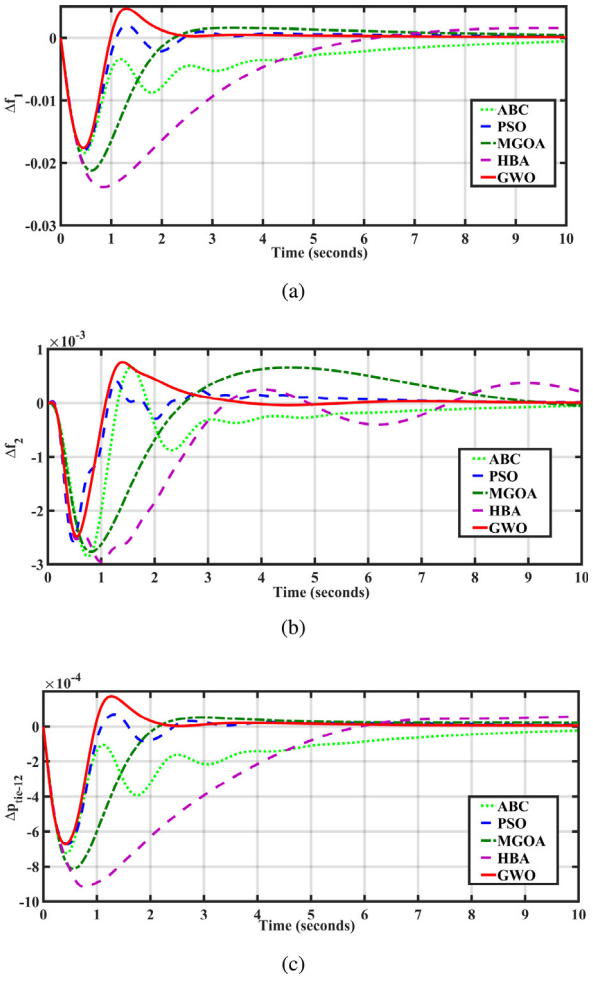


**Fig. 16.** (a) Frequency deviation in area-1; (b) Frequency deviation in area-2; (c) Tie-line Power deviation, with a 1% SLP within area-1 in system 1, incorporating non-linearity, for five different algorithms.

reaches a steady-state position more quickly and effectively than the other algorithms.

Additionally, Table 16 provides a comprehensive comparison of the four algorithms in terms of settling time ($T_s$), undershoot ($U_s$), overshoot ($O_s$), and ITAE for System 2. GWO again stands out with the lowest settling times of 12.9965 s, 14.0849 s, and 12.8183 s for $\Delta f_1$, $\Delta f_2$, and $\Delta p_{\text{tie12}}$, respectively. This is a marked improvement over the PSO algorithm, which has settling times of 15.1322 s, 13.3415 s, and 17.2145 s, and the ABC algorithm, which shows even higher settling times of 19.180 s, 18.9289 s, and 19.6621 s. Moreover, GWO demonstrates superior performance in terms of undershoot and overshoot, with values of −5.178 Hz, −1.819 Hz, and −1.095 Hz for undershoot, and 0.9929 Hz, 0.5415 Hz, and 0.4005 Hz for overshoot across $\Delta f_1$, $\Delta f_2$, and $\Delta p_{\text{tie12}}$. These values indicate a more stable and precise control response compared to PSO and ABC. The PSO algorithm exhibits higher undershoot and overshoot values, and the ABC algorithm performs the worst in these metrics, showing significant deviations.

**Table 15**
Parameter Gains and ITAE for different algorithms for system 2.

| Parameter | Algorithms | | |
|---|---|---|---|
| | GWO | PSO | ABC |
| $K_{X1}$ | 1.7784 | 1.5151 | 1.6054 |
| $K_{Y1}$ | 0.8516 | 0.3907 | 0.4898 |
| $K_{P1}$ | 1.3753 | 1.6551 | 1.1975 |
| $K_{I1}$ | 1.8299 | 1.0000 | 0.8959 |
| $K_{D1}$ | 0.8971 | 0.6959 | 0.9457 |
| $K_{X2}$ | 1.6193 | 1.2436 | 1.4350 |
| $K_{Y2}$ | 1.4240 | 0.2929 | 0.5979 |
| $K_{P2}$ | 1.5692 | 1.0088 | 1.3139 |
| $K_{I2}$ | 1.5085 | 0.8580 | 0.5543 |
| $K_{D2}$ | 0.8260 | 0.8194 | 0.4797 |
| $K_{X3}$ | 1.9106 | 1.1734 | 1.2895 |
| $K_{Y3}$ | 1.1648 | 0.5238 | 0.4323 |
| $K_{P3}$ | 1.4221 | 1.5652 | 1.6897 |
| $K_{I3}$ | 0.1010 | 0.1152 | 0.4390 |
| $K_{D3}$ | 1.3175 | 0.3552 | 0.8195 |
| ITAE | 0.0690 | 0.1138 | 0.3260 |

Overall, the GWO algorithm's low ITAE score of 0.0690, combined with its reduced settling times, undershoot, and overshoot values, highlights its effectiveness and efficiency in managing frequency and tie-line power deviations in System 2. This clearly positions GWO as the most favourable algorithm among those compared, offering enhanced control performance and precision.

## 5. Conclusion

This study developed a novel GWO-optimized fuzzy-PID controller, employing a triangular membership function, designed for load frequency control in a dual-area power system. The implementation utilized the Integral Time Absolute Error (ITAE) for parameter optimization, leading to marked performance enhancements. The analysis of different fuzzy membership functions — triangular, trapezoidal, and Gaussian — demonstrated that the triangular function provides superior control performance. Comprehensive assessments through sensitivity, non-linearity, random Step Load Perturbation (SLP) analyses, and stability analysis confirmed the controller's robustness and its capability to maintain stability under diverse disturbances. The integration of complex power generation systems, including thermal, hydro, and gas turbines with CES and HVDC links, further illustrates the controller's broad applicability. Despite its strengths, the study acknowledges limitations such as the exclusion of boiler dynamics and time delays in the analysis of non-linearity and stability, suggesting areas for future research. Extending this control approach to renewable-based power systems could offer insights into its adaptability in sustainable energy contexts. Comparatively, the GWO-based controller surpassed those based on Modified Grasshopper Optimization Algorithm (MGOA), Honey Badger Algorithm (HBA), Particle Swarm Optimization (PSO), Artificial Bee Colony (ABC), and Spider Monkey Optimization (SMO) across several metrics like ITAE, settling times, overshoot, and undershoot, highlighting its efficacy as a solution for modern power system challenges.

**Table 16**
Comparison analysis of dynamic performance metrics across different algorithms for system 2.

| Algorithm | $T_s$ (s) | | | $\lvert U_s \rvert$ (Hz) × $10^{-3}$ | | | $\lvert O_S \rvert$ (Hz) × $10^{-3}$ | | | ITAE |
|---|---|---|---|---|---|---|---|---|---|---|
| | $\Delta f_1$ | $\Delta f_2$ | $\Delta p_{tie-12}$ | $\Delta f_1$ | $\Delta f_2$ | $\Delta p_{tie-12}$ | $\Delta f_1$ | $\Delta f_2$ | $\Delta p_{tie-12}$ | |
| GWO | 12.9965 | 14.0849 | 12.8183 | −5.178 | −1.819 | −1.095 | 0.9929 | 0.5415 | 0.4005 | 0.0690 |
| PSO | 15.1322 | 13.3415 | 17.2145 | −5.178 | −1.817 | −1.261 | 1.004 | 0.4323 | 0.5099 | 0.1138 |
| ABC | 19.1800 | 18.9289 | 19.6621 | −5.5577 | −1.995 | −2.065 | 0.9241 | 0.3183 | 1.1250 | 0.3260 |

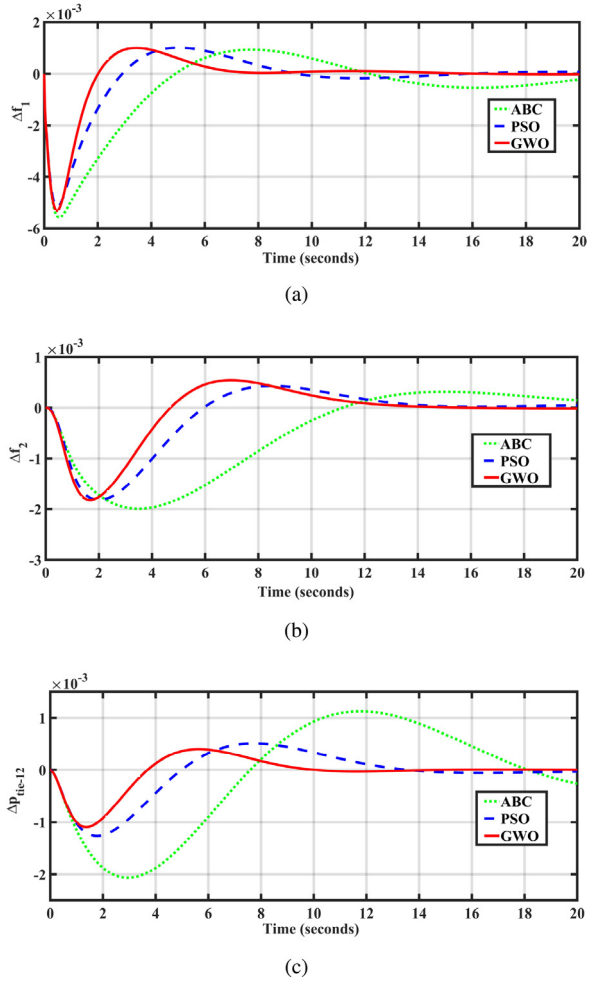


**Fig. 17.** (a) Frequency deviation in area-1; (b) Frequency deviation in area-2; (c) Tie-line Power deviation, with a 1% SLP within area-1 in system 2, incorporating non-linearity, using three different algorithms.

## CRediT authorship contribution statement

**Md. Faiyaj Ahmed Limon:** Writing – review & editing, Writing – original draft, Supervision, Software, Methodology, Investigation, Formal analysis, Conceptualization. **Rhydita Shahrin Upoma:** Writing – review & editing, Writing – original draft, Software, Formal analysis. **Nomita Sinha:** Writing – review & editing, Writing – original draft, Software, Formal analysis. **Shristi Roy Swarna:** Writing – review & editing, Writing – original draft, Software, Formal analysis. **Bidyut Kanti Nath:** Writing – review & editing, Writing – original draft, Methodology. **Kulsuma Khanum:** Writing – review & editing, Writing – original draft, Methodology. **Md. Jubaer Rahman:** Writing – review & editing, Writing – original draft, Methodology. **Md. Shahid Iqbal:** Writing – review & editing, Writing – original draft, Validation, Supervision, Methodology.

## Funding

No funding was received for this work.

## Declaration of competing interest

The authors declare that they have no known competing financial interests or personal relationships that could have appeared to influence the work reported in this paper.

## Acknowledgement

Nothing to declare.

## Data availability

Data will be made available on request.

## Appendix A

The parameters are: $f = 60$ Hz; $R_1 = R_2 = 2.4$ Hz/p.u; $T_{G1} = T_{G2} = 0.08$ s; $T_{T1} = T_{T2} = 0.3$ s; $B_1 = B_2 = 0.425$ p.u. MW/Hz; $T_{r1} = T_{r2} = 10$ s; $K_{r1} = K_{r2} = 0.5$; $T_{P1} = T_{P2} = 20$ s; $K_{P1} = K_{P2} = 120$ Hz/p.u. MW; $T_{12} = 0.545$; $a_{12} = -1$ [30].

## Appendix B

The parameters are: $T_{SG} = 0.08$ s; $T_T = 0.3$ s; $K_R = 0.3$; $T_R = 10$ s; $K_{PS1} = K_{PS2} = 68.9566$ Hz/p.u. MW; $T_{PS1} = T_{PS2} = 11.49$ s; $T_{12} = 0.0433$; $B_1 = B_2 = 0.4312$ p.u. MW/Hz; $P_{rt} = 2{,}000$ MW; $P_L = 1{,}840$ MW; $R_1 = R_2 = R_3 = 2.4$ Hz/p.u; $Y_C = 1$ s; $c_g = 1$; $b_g = 0.05$ s; $T_F = 0.23$ s; $T_{CR} = 0.01$ s; $T_{CD} = 0.2$ s; $K_T = 0.543478$; $K_H = 0.326084$; $K_G = 0.130438$; $K_{DC} = 1$; $T_{DC} = 0.2$ s; $a_{12} = -1$; $T_W = 1$ s; $T_{RS} = 5$ s; $T_{RH} = 28.75$ s; $T_{GH} = 0.2$ s; $X_C = 0.6$ s.

The CES data are: $T_1 = 0.279$ s; $T_2 = 0.026$ s; $T_3 = 0.411$ s; $T_4 = 0.1$ s; $K_{CES} = 0.3$; $T_{CES} = 0.0352$ s [7,34]

## References

[1] D.P. Kothari, I. Nagrath, Modern Power System Analysis, Tata McGraw-Hill Publishing Company, 2003.
[2] H. Shayeghi, H. Shayanfar, A. Jalili, Load frequency control strategies: A state-of-the-art survey for the researcher, Energy Convers. Manage. 50 (2) (2009) 344–353.
[3] M.N. Anwar, S. Pan, A new PID load frequency controller design method in frequency domain through direct synthesis approach, Int. J. Electr. Power Energy Syst. 67 (2015) 560–569.
[4] H. Saadat, et al., Power System Analysis, vol. 2, McGraw-Hill, 1999.
[5] K.S. Parmar, PSO based PI controller for the LFC system of an interconnected power system, Int. J. Comput. Appl. 88 (7) (2014).
[6] M.F. Ahmed Limon, M.F. Hasan Shiblee, A. Rouf, M.S. Iqbal, Hybrid ABC-PSO algorithm based static synchronous compensator for enhancing power system stability, in: 2023 10th IEEE International Conference on Power Systems, ICPS, 2023, pp. 1–6.
[7] M.S. Iqbal, M.F.A. Limon, M.M. Kabir, M.K.M. Rabby, M.J.A. Soeb, M.F. Jubayer, A hybrid optimization algorithm for improving load frequency control in interconnected power systems, Expert Syst. Appl. 249 (2024) 123702.
[8] E. Çelik, N. Öztürk, E.H. Houssein, Improved load frequency control of interconnected power systems using energy storage devices and a new cost function, Neural Comput. Appl. 35 (1) (2023) 681–697.

[9] S.A. Taher, M. Hajiakbari Fini, S. Falahati Aliabadi, Fractional order PID controller design for LFC in electric power systems using imperialist competitive algorithm, Ain Shams Eng. J. 5 (1) (2014) 121–135.
[10] N.E.Y. Kouba, M. Menaa, M. Hasni, M. Boudour, LFC enhancement concerning large wind power integration using new optimised PID controller and RFBs, IET Gener. Transm. Distrib. 10 (16) (2016) 4065–4077.
[11] B. Dhanasekaran, J. Kaliannan, A. Baskaran, N. Dey, J.M.R.S. Tavares, Load frequency control assessment of a PSO-PID controller for a standalone multi-source power system, Technologies 11 (1) (2023).
[12] P.P. Singh, R. Shankar, S. Singh, Chaos quasi-opposition crayfish based modified new controller designed for hybrid deregulated power environment considering cyber-attack, Chaos Solitons Fractals 187 (2024) 115444.
[13] H. Bevrani, T. Hiyama, Robust decentralised PI based LFC design for time delay power systems, Energy Convers. Manage. 49 (2) (2008) 193–204.
[14] P.K. Pathak, A.K. Yadav, Design of optimal cascade control approach for LFM of interconnected power system, ISA Trans. 137 (2023) 506–518.
[15] E. Çelik, Exponential PID controller for effective load frequency regulation of electric power systems, ISA Trans. 153 (2024) 364–383.
[16] M. Barakat, A. Donkol, H.F. Hamed, G.M. Salama, Harris hawks-based optimization algorithm for automatic LFC of the interconnected power system using PD-PI cascade control, J. Electr. Eng. Technol. 16 (2021) 1845–1865.
[17] E. Çelik, N. Öztürk, Y. Arya, C. Ocak, (1+PD)-PID cascade controller design for performance betterment of load frequency control in diverse electric power systems, Neural Comput. Appl. 33 (22) (2021) 15433–15456.
[18] M.S. Iqbal, M.F.A. Limon, M.M. Kabir, M.Z. Hossain, M.F. Jubayer, M.J.A. Soeb, A hybrid optimization algorithm based on cascaded (1 + PI)-PI-PID controller for load frequency control in interconnected power systems, Results Eng. 24 (2024) 103624.
[19] E. Çelik, N. Öztürk, Novel fuzzy 1PD-TI controller for AGC of interconnected electric power systems with renewable power generation and energy storage devices, Eng. Sci. Technol. Int. J. 35 (2022) 101166.
[20] U. Raj, R. Shankar, Optimally enhanced fractional-order cascaded integral derivative tilt controller for improved load frequency control incorporating renewable energy sources and electric vehicle, Soft Comput. 27 (20) (2023) 15247–15267.
[21] M. El-Sherbiny, G. El-Saady, A.M. Yousef, Efficient fuzzy logic load–frequency controller, Energy Convers. Manage. 43 (14) (2002) 1853–1863.
[22] H. Shayeghi, A. Jalili, H. Shayanfar, Multi-stage fuzzy load frequency control using PSO, Energy Convers. Manage. 49 (10) (2008) 2570–2580.
[23] C.-F. Juang, C.-F. Lu, Load-frequency control by hybrid evolutionary fuzzy PI controller, IEE Proc. Gener. Transm. Distrib. 153 (2) (2006) 196–204.
[24] B.K. Sahu, T.K. Pati, J.R. Nayak, S. Panda, S.K. Kar, A novel hybrid LUS–TLBO optimized fuzzy-PID controller for load frequency control of multi-source power system, Int. J. Electr. Power Energy Syst. 74 (2016) 58–69.
[25] P. Jood, S. Aggarwal, V. Chopra, Performance assessment of a neuro-fuzzy load frequency controller in the presence of system non-linearities and renewable penetration, Comput. Electr. Eng. 74 (2019) 362–378.
[26] B. Khokhar, S. Dahiya, K.S. Parmar, A novel hybrid fuzzy PD-TID controller for load frequency control of a standalone microgrid, Arab. J. Sci. Eng. 46 (2021) 1053–1065.
[27] R. Khezri, S. Golshannavaz, S. Shokoohi, H. Bevrani, Fuzzy logic based fine-tuning approach for robust load frequency control in a multi-area power system, Electr. Power Compon. Syst. 44 (18) (2016) 2073–2083.
[28] G. Chen, Z. Li, Z. Zhang, S. Li, An improved ACO algorithm optimized fuzzy PID controller for load frequency control in multi area interconnected power systems, IEEE Access 8 (2020) 6429–6447.
[29] E. Çelik, Performance analysis of SSA optimized fuzzy 1PD-PI controller on AGC of renewable energy assisted thermal and hydro-thermal power systems, J. Ambient Intell. Humaniz. Comput. 13 (8) (2022) 4103–4122.
[30] D. Tripathy, A.K. Barik, N.B.D. Choudhury, B.K. Sahu, Performance comparison of SMO-based fuzzy PID controller for load frequency control, in: J.C. Bansal, K.N. Das, A. Nagar, K. Deep, A.K. Ojha (Eds.), Soft Computing for Problem Solving, Springer Singapore, Singapore, 2019, pp. 879–892.
[31] K. Rajesh, S. Dash, Load frequency control of autonomous power system using adaptive fuzzy based PID controller optimized on improved sine cosine algorithm, J. Ambient Intell. Humaniz. Comput. 10 (2019) 2361–2373.
[32] P.C. Sahu, R.C. Prusty, B. Sahoo, Modified sine cosine algorithm-based fuzzy-aided PID controller for automatic generation control of multiarea power systems, Soft Comput. 24 (17) (2020) 12919–12936.
[33] A. Dutta, S. Prakash, Load frequency control of multi-area hybrid power system integrated with renewable energy sources utilizing FACTS & energy storage system, Environ. Prog. Sustain. Energy 39 (2) (2020) e13329.
[34] R.K. Khadanga, A. Kumar, Analysis of PID controller for the load frequency control of static synchronous series compensator and capacitive energy storage source-based multi-area multi-source interconnected power system with HVDC link, Int. J. Bio-Inspir. Comput. 13 (2) (2019) 131–139.
[35] M.K. Debnath, T. Jena, S.K. Sanyal, Frequency control analysis with PID-fuzzy-PID hybrid controller tuned by modified GWO technique, Int. Trans. Electr. Energy Syst. 29 (10) (2019) e12074.
[36] B. Sahoo, S. Panda, Improved grey wolf optimization technique for fuzzy aided PID controller design for power system frequency control, Sustain. Energy Grids Netw. 16 (2018) 278–299.
[37] R.K. Sahu, S. Panda, P.C. Pradhan, Design and analysis of hybrid firefly algorithm-pattern search based fuzzy PID controller for LFC of multi area power systems, Int. J. Electr. Power Energy Syst. 69 (2015) 200–212.
[38] B.K. Sahu, S. Pati, S. Panda, Hybrid differential evolution particle swarm optimisation optimised fuzzy proportional–integral derivative controller for automatic generation control of interconnected power system, IET Gener. Transm. Distrib. 8 (11) (2014) 1789–1800.
[39] S. Mirjalili, S.M. Mirjalili, A. Lewis, Grey wolf optimizer, Adv. Eng. Softw. 69 (2014) 46–61.
[40] S.M. Dubey, H.M. Dubey, S.R. Salkuti, Modified quasi-opposition-based grey wolf optimization for mathematical and electrical benchmark problems, Energies 15 (15) (2022).
[41] D. Izci, S. Ekinci, E. Çelik, M. Bajaj, V. Blazek, L. Prokop, Dynamic load frequency control in power systems using a hybrid simulated annealing based quadratic interpolation optimizer, Sci. Rep. 14 (1) (2024) 26011.
[42] S. Gouran-Orimi, A. Ghasemi-Marzbali, Load frequency control of multi-area multi-source system with nonlinear structures using modified grasshopper optimization algorithm, Appl. Soft Comput. 137 (2023) 110135.
[43] S. Ozumcan, A. Ozturk, M. Varan, C. Andic, A novel honey badger algorithm based load frequency controller design of a two-area system with renewable energy sources, Energy Rep. 9 (2023) 272–279, The 8th International Conference on Sustainable and Renewable Energy Engineering.

**Md. Faiyaj Ahmed Limon** is currently a Lecturer in the Department of Electrical and Electronic Engineering at Leading University, Bangladesh. He earned his Bachelor's degree in Electrical and Electronic Engineering from Sylhet Engineering College, affiliated with Shahjalal University of Science and Technology (SUST), in 2023. His research interests include optimization algorithms, control strategies, and machine learning applications in power systems, with a focus on load frequency control and renewable energy integration. Faiyaj has developed modified hybrid algorithms for load frequency control and has been a Research Assistant at Sylhet Engineering College since 2022. He is actively involved in designing innovative controllers for photovoltaic systems and enhancing image quality using convolutional neural networks. Additionally, he is interested in pursuing further studies in power system stability, algorithms, optimization, and machine learning.

**Rhydita Shahrin Upoma** received her B.Sc. degree in Electrical and Electronic Engineering from Sylhet Engineering College, affiliated with Shahjalal University of Science and Technology (SUST), in 2024. Her research interests include power system analysis and control, with a focus on Fuzzy Logic and its applications, complex load frequency control (LFC) systems, PV inverters, and boost converters. Additionally, she explores the implementation of advanced algorithms such as Grey Wolf Optimizer (GWO), Artificial Bee Colony (ABC), and Particle Swarm Optimization (PSO) to improve the efficiency and stability of LFC systems in modern power grids. She is dedicated to advancing renewable energy integration through innovative control strategies.

**Nomita Sinha** received her B.Sc. in Electrical and Electronic Engineering from Sylhet Engineering College, affiliated with Shahjalal University of Science and Technology (SUST), Bangladesh, in 2024. Her research interests span Power Systems, Fuzzy Logic, Energy Economics, and Artificial Intelligence (AI). She is particularly focused on integrating fuzzy logic and AI to optimize energy systems and enhance decision-making in power system operations. Nomita is also exploring the economic implications of renewable energy sources and their impact on the power grid, aiming to develop innovative, sustainable solutions for future energy challenges.

**Shristi Roy Swarna** received her B.Sc. in Electrical and Electronic Engineering from Sylhet Engineering College, affiliated with Shahjalal University of Science and Technology (SUST) Bangladesh, in 2024. Her current research interests encompass Power Systems, Electrical Machines, and Communication Systems. She has also explored topics such as renewable energy integration and smart grid technologies, focusing on improving system efficiency and stability. In addition to her academic work, Shristi is involved in collaborative research on machine learning applications in power grid management, aiming to enhance the resilience and adaptability of modern power networks.

**Bidyut Kanti Nath** Nath received his B.Sc. degree in Electrical and Electronic Engineering from Sylhet Engineering College, affiliated with Shahjalal University of Science and Technology (SUST), in 2023. He is currently a Lecturer in the Department of Electrical and Electronic Engineering at Leading University, Sylhet, Bangladesh. His research interests focus on power system analysis and control and distributed control. He is actively involved in studying advanced techniques to enhance the efficiency and reliability of power systems, aiming to contribute to the modernization of energy networks.

**Kulsuma Khanum** is a Lecturer in the Department of Electrical and Electronic Engineering (EEE) at Leading University, Sylhet, Bangladesh. She received Bachelor's degree in Electrical and Electronic Engineering from Sylhet Engineering College, affiliated with Shahjalal University of Science and Technology (SUST), in 2023. Her research focuses on renewable energy, energy efficiency, and grid integration, particularly in the context of electric vehicle charging technology and smart grid systems. Kulsuma is dedicated to driving innovations that contribute to a more sustainable and resilient energy future through advanced grid solutions.

**Md. Jubaer Rahman** received his B.Sc. degree in Electrical and Electronic Engineering from Sylhet Engineering College, Shahjalal University of Science and Technology, Sylhet, Bangladesh, in 2021. He is currently pursuing his master's degree in Electrical and Electronic Engineering at Dhaka University of Engineering and Technology (DUET), Gazipur, Bangladesh. In addition, he works as an Assistant Engineer at the 114 MW Feni Lanka Power Limited. He has also served as a Research Assistant at the DUET High Voltage Lab. His research interests include power system optimization, dielectrics, and clean energy systems.

**Md. Shahid Iqbal** is an Assistant Professor and Head of the Department of Electrical and Electronic Engineering at Sylhet Engineering College. He holds a B.Sc. in Electrical and Electronic Engineering from Khulna University of Engineering and Technology (KUET) and an M.Sc. from Dhaka University of Engineering and Technology (DUET). Currently pursuing a Ph.D. at DUET, his research spans Artificial Intelligence, Machine Learning, Deep Learning, and Renewable Energy, with several published papers in these fields. In addition to his technical expertise, he is deeply involved in Education Research, focusing on curriculum development and enhancing learning experiences in engineering education. He has also worked on various collaborative projects aimed at integrating AI techniques into energy systems to improve efficiency and sustainability.